Nonadiabatic Trajectory Studies of $NaI(H_2O)_n$ Photodissociation Dynamics†

Denise M. Koch,‡ Qadir K. Timerghazin,‡ Gilles H. Peslherbe,*,‡ Branka M. Ladanyi,§ and James T. Hynes#

Centre for Research in Molecular Modeling and Department of Chemistry & Biochemistry, Concordia University, Montréal, Québec, Canada H4B 1R6, Department of Chemistry, Colorado State University, Fort Collins, Colorado 80523, Département de Chimie, Ecole Normale Supérieure, UMR 8640 PASTEUR, 24 rue Lhomond, 75213 Paris, France, and Department of Chemistry & Biochemistry, University of Colorado, Boulder, Colorado 80309-0215

Received: August 19, 2005; In Final Form: November 17, 2005

We have investigated the photodissociation dynamics of $NaI(H_2O)_n$ [$n = 1-4$] clusters using the molecular dynamics with quantum transitions method and a quantum mechanics/molecular mechanics description of $NaI(H_2O)_n$, which involves a semiempirical valence-bond approach to describe the NaI electronic structure and classical solvent−solvent and solute−solvent interaction potentials. Our simulation results show that the $NaI(H_2O)_n$ excited-state population decay upon reaching the NaI curve-crossing region increases with cluster size due to the stabilization of the ionic branch of the NaI excited state by the surrounding water molecules, and the resulting increase in nonadiabatic transition probability. After reaching the curve-crossing region for the first time, however, the excited-state population decay resembles that of bare NaI because of rapid evaporation of 99% and 95% of the water molecules for $NaI(H_2O)$ and $NaI(H_2O)_n$ [$n = 2-4$], respectively. This extensive evaporation is due to the reversed NaI polarity in the Franck−Condon region of the NaI first excited state, which causes strong repulsive $NaI-H_2O$ forces and induces rapid nonstatistical water evaporation, where product water molecules are formed more rotationally than translationally hot. A few water molecules (5% or less) remain transiently or permanently bound to NaI, forming long-lived clusters, when NaI remains predominantly ionic, i.e., remains in the excited state, after reaching the curve-crossing region. To connect simulation results with experiment, we have simulated femtosecond probe signals resulting from two-photon and one-photon excitation to the X and I NaI^+ probe states. In agreement with experimental findings, the probe signals resulting from the two-photon probe scheme, where excitation occurs from the covalent branch of the excited state, decay exponentially over the NaI first excited-state vibrational period, with very little evidence of long-time dynamics. The one-photon probe scheme (not used for experimental cluster studies) is shown to be less sensitive to solvation, in that excitation energies will remain similar over a range of cluster sizes, as the ionic branch of the excited state and the NaI^+ probe states are stabilized to the same extent by the presence of water molecules. The resulting probe signals are also more revealing of the $NaI(H_2O)_n$ photodissociation dynamics than the two-photon probe signals, as they may allow monitoring of solvation effects on the NaI nonadiabatic dynamics and of successive evaporation of water molecules. Time-resolved photoelectron spectra provide limited additional information regarding the $NaI(H_2O)_n$ photodissociation dynamics. A key consequence of the rapid water evaporation demonstrated here is that experimentally observed signals may arise from the photodissociation of much larger $NaI(H_2O)_n$ parent clusters.

I. Introduction

The electronic structure of alkali-metal halides is characterized by a crossing of covalent and ionic curves, or equivalently an avoided crossing between ground and excited-state adiabatic curves which change their electronic character in the neighborhood of the avoided crossing.[1] This characteristic leads to interesting effects in their dissociation dynamics and has prompted a number of experimental and theoretical studies of their gas-phase photodissociation dynamics, especially for NaI.[1−11] The latter has attracted much attention because it is one of the alkali-metal halides with the smallest internuclear separation at which the ionic and covalent curves cross.[1] At small internuclear separations, the electronic coupling between the diabatic states is large enough to enable the resulting adiabatic potentials to govern, at least in part, the nuclear motion. At large separations, this coupling is exponentially small and the dissociation proceeds nonadiabatically, as if there were no mixing of the covalent and ionic configurations.[12]

The gas-phase photodissociation of NaI has been extensively investigated with femtosecond transition-state spectroscopy,[5,6,13] and experimental results have been successfully compared to quantum mechanical, semiclassical and classical calculations.[5,7,10] In typical experiments, excitation from the ground (ionic) $^1\Sigma^+$ state to both the excited adiabatic $\Omega = 1$ and $\Omega = 0^+$ states (which are essentially covalent in the Franck−Condon region) are possible, and ionic products are not energetically accessible.[7] Due to symmetry considerations, the $\Omega = 1$ state has no ionic character at any separation and, because it is purely

† Part of the special issue "William Hase Festschrift".

* Corresponding author. E-mail: ghp@alcor.concordia.ca. Tel.: (514) 848-2424 ext. 3335. Fax: (514) 848-2868.

‡ Concordia University.

§ Colorado State University.

Ecole Normale Supérieure and University of Colorado.

10.1021/jp054692v CCC: $33.50
Published on Web 01/26/2006

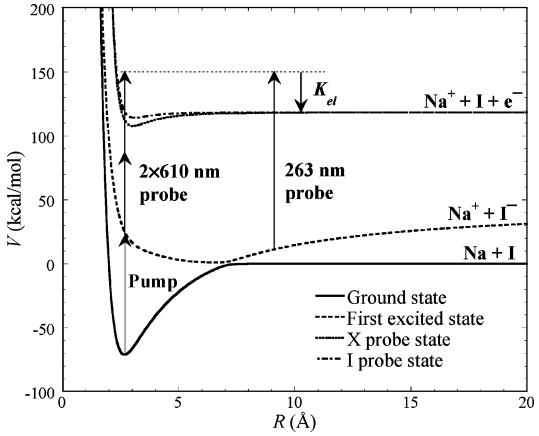

Figure 1. NaI potential energy curves for the ground and first excited adiabatic states, and the X and I probe states. Also illustrated are the one-photon (263 nm) and two-photon (2×610 nm) probe schemes employed to generate simulated probe signals, and the electron kinetic energy K_{el} that is evaluated to generate time-resolved photoelectron spectra.

repulsive and does not predissociate,[14] the NaI molecules excited to this state produce free atoms on a very short time scale. On the other hand, the NaI molecules excited to the $\Omega = 0^+$ state, whose character is covalent in the Franck−Condon region but ionic at larger separations, exhibit more interesting dynamics: they may be transiently trapped in a well formed by the avoided crossing of the covalent 0^+ and ionic surfaces, and then undergo a nonadiabatic transition to form atomic products.[5,6] The excited-state population evolution can be followed in time by promoting the freshly excited NaI to a probe state, as depicted in Figure 1, whose population can in turn be monitored by laser-induced fluorescence of the sodium D line[5,6] or by collection of sodium ions by mass spectrometry.[15] These detection schemes give rise to oscillatory signals (because of the transient trapping of the NaI population in the excited-state well) with decreasing amplitude, because of the leakage of excited-state population to form atoms via nonadiabatic transitions.

Our own interest in NaI has centered on the photodissociation dynamics for this system in solution[16] and in clusters.[17] Polar solvent molecules preferentially stabilize molecular species with a localized charge character, and ionic products of alkali-metal halide photodissociation may become more favorable in solution or in small clusters. More generally, polar and/or polarizable solvents are known to modify solute electronic structures and influence the dynamics of chemical reactions, and we are particularly interested in the influence of solvation on the curve crossing dynamics of the NaI paradigm molecule. Our earlier theoretical work on NaI in solution,[16] which employed a combination of semiempirical valence bond theory in solution developed by Hynes and co-workers[18,19] and transition-state theory,[20] showed that activated electron transfer (ET) would occur on the millisecond time scale. Remarkably, NaI was predicted to undergo electron transfer in the inverted regime.[21] Unfortunately, radiative deactivation of the freshly excited NaI followed by recombination of the ions on the ground-state surface occurs on the nanosecond time scale and would short-circuit any electron transfer process. This work also suggested that activated ET might occur in small clusters, which are sufficiently large to involve significant solvation and "solvent" reorganization, but sufficiently small so that the associated ET barrier would be low enough to allow competition with radiative decay to an environmentally stabilized ground ionic state.

Cluster studies are also of independent fundamental interest and have been the subject of recent experiments[22−24] motivated in part by our earlier theoretical work,[17] which showed how the presence of a single solvent molecule affects the nonadiabatic dynamics of NaI photodissociation. In experimental studies of NaI ion pairs in polar solvent clusters of water, acetonitrile, and ammonia,[22−24] a very clear solvent-selective behavior was observed in the distribution of the detected $Na^+(solvent)_n$ product ions.[22] For instance, clusters of size up to $n \sim 50$ have been observed experimentally with water, but no clusters larger than sizes 10 and 7 have been observed with ammonia and acetonitrile, respectively.[22] In previous theoretical work, we also investigated the structure and thermodynamics of NaI ion pairs in aqueous clusters.[25,26] We found that NaI ion pairs are actually stable with respect to complete ground-state dissociation, even in very large water clusters, but that solvent-separated ion pairs (SSIP) become rapidly predominant over contact ion pairs (CIP) with increasing cluster size. Model electronic structure calculations showed that SSIP have a much reduced oscillator strength and may not possess optically accessible excited states akin to that of gas-phase NaI.[25] Our findings are consistent with the fact that products of $NaI(H_2O)_n$ cluster photodissociation of size $n > 50$ were not observed experimentally, as the larger SSIP parent clusters may just not be photochemically active. Interestingly enough, we also found that the structure of ion pairs in water clusters could be relatively simply related to that of the individual ions in water clusters.[26] Of particular importance in this case is the now well-known hydration structure of the iodide ion in aqueous clusters,[27−29] in which iodide preferentially sits at the surface of small- to medium-sized clusters, a solvation character that may explain why NaI ion pairs are "dragged" to the surface of small water clusters.[26] Recently, Jungwirth and Tobias demonstrated that large halide ions tend to accumulate at the surface of the air/water interface of alkali-metal halide solutions for similar reasons, a finding which is of great importance for heterogeneous atmospheric chemistry.[30]

A striking finding in our earlier theoretical work[17] was the importance of solvent evaporation in the $NaI(H_2O)$ photodissociation dynamics. Because it obviously significantly decreases the size of the cluster being investigated in the course of the reaction, one needs to pay attention to larger parent clusters to attempt a connection with experimental results, which have been primarily reported for the (product) cluster size range $n = 1-8$.[24] One objective of the present work is to assess the importance of solvent evaporation in the photodissociation dynamics of $NaI(H_2O)_n$ [$n > 1$] clusters to make a more thorough connection with experimental findings. Another equally important objective is to investigate the nonadiabatic dynamics of photodissociation (and electron transfer) in $NaI(H_2O)_n$ clusters as a function of cluster size and to simulate femtosecond probe signals and time-resolved photoelectron spectra for possible connection with experiment. As the differential solvation between the ionic and covalent NaI states increases with cluster size, one might expect different nonadiabatic transition dynamics as the ionic state becomes increasingly more stabilized upon addition of water molecules.

The outline of this article is as follows. The semiempirical valence-bond theory employed to describe the NaI electronic structure, the interaction potentials and the simulation methodology are presented in section II. The results of the simulations are presented in section III, where particular attention is paid to water evaporation, nonadiabatic dynamics and possible connection with experiment. Concluding remarks follow in section IV.

II. Computational Methodology

A. QM/MM Potential Energy Surfaces. In this work, we adopt a quantum mechanical/molecular mechanical (QM/MM) description of the $NaI(H_2O)_n$ system, where the NaI solute is treated with semiempirical valence-bond (VB) theory and the water solvent molecules are described by classical model potentials. The total system Hamiltonian is

$$\hat{H}_T = \hat{K}_R + \hat{K}_{R^S} + \hat{H}(\mathbf{R},\mathbf{r},\mathbf{R}^s) + \hat{V}(\mathbf{R},\mathbf{R}^s) \quad (1)$$

where $\mathbf{R}$ and $\mathbf{R}^s$ represent the nuclear degrees of freedom of the NaI solute and the solvent molecules, respectively, and $\mathbf{r}$ is the NaI solute electronic degrees of freedom. The first two terms in the Hamiltonian of eq 1 are the nuclear kinetic energies, the third term is the Hamiltonian for the NaI electronic structure and the last term represents the classical potential of the solvent molecules, including interactions with the solute nuclei. The solute Hamiltonian can be written as

$$\hat{H}(\mathbf{R},\mathbf{r},\mathbf{R}^s) = \hat{H}^0(\mathbf{R},\mathbf{r}) + \hat{V}^C(\mathbf{R},\mathbf{r},\mathbf{R}^s) \quad (2)$$

where $\hat{H}^0(\mathbf{R},\mathbf{r})$ is the solute gas-phase Hamiltonian (excluding the nuclear kinetic energy) and $\hat{V}^C(\mathbf{R},\mathbf{r},\mathbf{R}^s)$ represents the Coulombic interaction between the solvent molecule charge distribution and the solute electronic degrees of freedom. With this ansatz, it is obvious that the solvent is allowed to affect the electronic structure of the solute via electrostatic interactions. Finally, the last term of the Hamiltonian in eq 1 is expressed as

$$\hat{V}(\mathbf{R},\mathbf{R}^s) = \hat{V}^C_{ss}(\mathbf{R}^s) + \hat{V}^{r-d}_{ss}(\mathbf{R}^s) + \hat{V}^{r-d}(\mathbf{R},\mathbf{R}^s) \quad (3)$$

where the first two terms are the solvent−solvent Coulombic and repulsion−dispersion interactions and the last term represents the repulsion−dispersion interaction between the nuclei of the solute and those of the solvent molecules.

1. NaI Electronic Structure and Potentials. The NaI electronic structure is expressed as a linear combination of ionic and covalent charge-localized VB (or diabatic) states

$$\psi = \sum c_i \Phi_i \quad (4)$$

and the wave function is solved for in the framework of semiempirical VB theory.[16,31,32] In this theory, some or all of the valence electrons are treated explicitly, whereas all other solute electronic and nuclear energy contributions are embedded in a core−core potential H^{cc}. One-electron and two-electron integrals for the electrons treated explicitly are evaluated using semiempirical expressions, based on the point charge, Pariser and Mulliken approximations,[33] resulting in analytical expressions for all diabatic matrix elements.

For alkali-metal halides MX, only two electrons need to be considered explicitly[16] and the charge-localized VB states are expressed as the normalized Slater determinants $\Phi_1 = N_1|\bar{X}X|$ and $\Phi_2 = N_2(|\bar{M}X| - |M\bar{X}|)$ for the ionic and covalent states, respectively, where the core electrons have been omitted, X represents the halogen valence p orbital lying along the bond axis, and M represents the alkali-metal valence s orbital. The corresponding vacuum electronic Hamiltonian matrix elements, which represent the diabatic ionic and covalent curves, are given by[16]

$$H^0_{11}(R) = \langle\Phi_1|\hat{H}^0|\Phi_1\rangle = H^{cc}(R) - \mathrm{IP(X)} - \mathrm{EA(X)} - \frac{2e^2}{R} \quad (5)$$

$$H^0_{22}(R) = \langle\Phi_2|\hat{H}^0|\Phi_2\rangle = \frac{1}{2[1+S_{MX}{}^2(R)]}\left\{H^{cc}(R) - 2\mathrm{IP(X)} - 2\mathrm{IP(M)} - \frac{2e^2}{R}\right\} - \frac{S_{MX}{}^2(R)}{1+S_{MX}{}^2(R)}\left\{3\mathrm{IP(X)} + 3\mathrm{IP(M)} + \mathrm{EA(X)} + \mathrm{EA(M)} + \frac{2e^2}{R} + 2\rho(\mathrm{X}) + 2\rho(\mathrm{M})\right\} \quad (6)$$

with the electronic coupling

$$H^0_{12}(R) = \langle\Phi_1|\hat{H}^0|\Phi_2\rangle = \frac{S_{MX}(R)}{\sqrt{2[1+S_{MX}{}^2(R)]}}\left\{2H^{cc}(R) - 2\mathrm{IP(X)} - \mathrm{IP(M)} - \mathrm{EA(X)} - \frac{2e^2}{R} - \frac{1}{2}\rho(\mathrm{X}) - \frac{1}{2}\rho(\mathrm{M})\right\} \quad (7)$$

whereas the diabatic-state overlap is

$$S_{12}(R) = \langle\Phi_1|\Phi_2\rangle = \frac{S_{MX}(R)}{\sqrt{2[1+S_{MX}{}^2(R)]}} \quad (8)$$

where R is the internuclear separation, IP and EA are the ionization potential and electron affinity, ρ(X) is a one-electron integral of the form $\langle X|1/r|X\rangle$ and S_{MX} is the overlap between the metal s and halogen p orbital. For Slater orbitals,[34,35] ρ is just the Slater exponent ξ divided by the principal quantum number n and the overlap S_{MX} can be calculated analytically in terms of auxiliary functions.[36] The 5p Slater orbital with exponent $\xi = 1.9$ and the 3s Slater orbital with exponent $\xi = 0.7333$ are used here for iodine and sodium, respectively.[34,35] The ionization potentials for sodium and iodine are 5.14 and 10.45 eV, respectively, and the electron affinities of sodium and iodine are 0.55 and 3.06 eV, respectively.[37]

In the present work and in contrast to our earlier work,[16] we slightly depart from the original semiempirical theory and adjust the core−core potential parameters separately for both VB states to better reproduce experimentally derived potentials and experimental Franck−Condon (FC) energy gaps. $H^{cc}_{11}(R)$ is chosen so as to match the ionic diabatic-state energy $H^0_{11}(R)$ with the widely accepted ionic potential due to Levine and coworkers,[4] whose functional form is a slightly modified form of the Rittner potential,[38] i.e.

$$H^{cc}_{11}(R) = \mathrm{IP(X)} + \mathrm{IP(M)} + \left[A_{ion} + \left(\frac{B_{ion}}{R}\right)^8\right]e^{-R/R_{ion}} + \frac{e^2}{R} + E_{vdw/pol}(R) \quad (9)$$

where the van der Waals attraction and polarization energy term is expressed as

$$E_{vdw/pol}(R) = -\frac{C_{vdw}}{R^6} - \frac{(\alpha_{M^+} + \alpha_{X^-})e^2}{2R^4} - \frac{(2\alpha_{M^+}\alpha_{X^-})e^2}{R^7} \quad (10)$$

with $A_{ion} = 2760$ eV, $B_{ion} = 2.398$ eV$^{1/8}$Å, $R_{ion} = 0.3489$ Å, $C_{vdw} = 11.3$ eV·Å,[6] $\alpha_{M^+} = 0.408$ Å^3 and $\alpha_{X^-} = 6.431$ Å^3.[4,39] There have been a number of experimental studies aimed at characterizing the covalent state.[14,39−42] With a core−core potential of the form

$$H^{cc}_{22}(R) = \mathrm{IP(X)} + \mathrm{IP(M)} + A_{cov}e^{-B_{cov}(R-R_{cov})} \quad (11)$$

where $A_{cov} = 0.8$ eV, $B_{cov} = 2.5$ Å^{-1} and $R_{cov} = 2.65$ Å, the covalent-state potential matches covalent curves derived from total absorption spectra[14] and is very similar to potentials recently derived from various experiments.[40,43] The position of the covalent repulsive wall that we have determined coincides with the one used by Zewail and co-workers for their classical and quantum mechanical calculations.[5,7]

With the latter parametrization of the core−core potentials, the position of the covalent and ionic curve crossing determined here, $R_c \sim 7$ Å, is in good agreement with the commonly accepted value 6.93 Å.[1] The diabatic-state electronic resonance coupling $H_{12}^0(R)$, obtained from the semiempirical VB calculations appears to have a more reasonable behavior than that of Zewail and co-workers,[5,7] in that it is exponential in the internuclear separation range $R > 2.7$ Å, in agreement with ab initio calculations.[11] The semiempirical VB theory value −0.06 eV of $H_{12}^0(R)$ at the crossing point is in rather good agreement with the accepted value −0.055 eV, for which there is a wide consensus, both theoretically and experimentally.[5,12,39,40]

The secular equation is solved next for the two-state problem to yield the NaI adiabatic electronic ground ($X^1\Sigma^+$) and first excited ($A^1\Sigma^+$) states. The potential energy curves for both adiabatic states (cf. Figure 1) are in good agreement with multireference singly and doubly excited configuration interaction (MRCI) ab initio calculations by Sakai et al.,[9] and more recent ones by Alekseyev et al. that include spin−orbit coupling.[11] As expected, the first excited state exhibits a shallow well resulting from the avoided crossing of the ionic and covalent states. The gas-phase NaI Franck−Condon (FC) excitation energy predicted by our semiempirical VB model corresponds to a wavelength of 296 nm, which lies at the lower end of the experimental range of excitation wavelengths.[5,6] For instance, the calculated FC excess energy in the excited adiabatic state is 4−8 kcal/mol larger than its experimental counterpart for typical experiments carried out at 300 and 312 nm, respectively.[5,6,15] Overall, the NaI potentials are in reasonable agreement, not only with experiment but also with high-level ab initio calculations.[9,11]

2. Solvation and Water Potentials. The ionic−covalent electronic coupling is small in the neighborhood of the diabatic curve crossing (less than 2 kcal/mol), which is indicative of the Born−Oppenheimer regime of solvation,[16] where the solvent electrons move much faster than the solute electrons, so that the solvent effectively "feels" charge-localized solute-state charge distributions. As a result, following our earlier work,[16,44] the instantaneous solvation energy for the solute VB-state charge distributions is computed and incorporated in the individual Hamiltonian matrix elements, i.e.

$$H_{ij} = H_{ij}^0 + V_{ij}^C \tag{12}$$

before solving for adiabatic energies. By using the point-charge approximation embedded in semiempirical VB theory, the diagonal Coulombic interaction matrix elements become

$$V_{ii}^C = \sum_j \frac{q_{Na}^i q_j^s}{|\mathbf{R}_{Na} - \mathbf{R}_j^s|} + \sum_j \frac{q_I^i q_j^s}{|\mathbf{R}_I - \mathbf{R}_j^s|} \tag{13}$$

where j labels the charge sites of solvent molecules (the s superscript refers to solvent molecules), and q_{Na}^i and q_I^i represent the sodium and iodine charges in the ith diabatic state, respectively. Finally, the Coulomb-matrix off-diagonal elements are estimated via the Mulliken approximation

$$V_{ij}^C = \frac{S_{ij}}{2}(V_{ii}^C + V_{jj}^C) \tag{14}$$

This level of description of the solute−solvent electrostatic interactions in terms of point charges is in complete agreement with the spirit of the semiempirical VB theory used to describe the NaI electronic structure.

The sodium and iodine charges are obtained from a fit of the MRCI ground and first excited-state NaI dipole moments as a function of NaI internuclear separation.[9] We note that, even though fixed gas-phase charge distributions are employed for the NaI diabatic states, the solvent polarizes NaI by modifying the contribution of each VB state to the NaI electronic structure. A very interesting feature of the dipole moment curves is that the first excited state is polarized in the Franck−Condon region, but with a reverse polarity, compared to that of the ionic ground state. For example, the apparent partial charges of $Na^+\delta I^{-\delta}$ are +0.75 and −0.35 for the ground and excited adiabatic NaI states in the FC region, respectively. This finding, which appears to be characteristic of alkali-metal halides, can be interpreted in light of semiempirical VB theory and the classical model of polarization that is embedded in the core−core potential to correct for the minimum basis set deficiency of semiempirical theory, as discussed earlier.[17] The latter finding, as we shall see shortly, has a dramatic impact on the $NaI(H_2O)_n$ photodissociation mechanism and dynamics, just as was found previously for $NaI(H_2O)$.[16]

The water is described by the rigid TIP4P model,[45] which consists of Coulombic potentials for electrostatic interactions [$\hat{V}_{ss}^C(\mathbf{R}^s)$ in eq 3], using point charges of $+0.52e$ on the hydrogen atoms and $-1.04e$ on an interaction site situated on the bisector of the H−O−H angle at 0.15 Å from the oxygen atom, and parametrized Lennard-Jones functions for repulsion−dispersion interactions [$\hat{V}_{ss}^{r-d}(\mathbf{R}^s)$ in eq 3] with parameters $\epsilon_{O-O} = 0.155$ kcal/mol and $\sigma_{O-O} = 3.154$ Å. The nonelectrostatic part of the NaI−water interactions [$\hat{V}^{r-d}(\mathbf{R},\mathbf{R}^s)$ in eq 3] is described by Lennard-Jones terms such as for OPLS potentials.[46] The parameters for Na^+-H_2O interactions ($\epsilon_{O-Na} = 0.499$ kcal/mol and $\sigma_{O-Na} = 2.446$ Å) are taken from the early work of Jorgensen and co-workers,[47] whereas the parameters for $I-H_2O$ interactions ($\epsilon_{O-I} = 0.225$ kcal/mol and $\sigma_{O-I} = 3.970$ Å), which have not been reported to our knowledge, were derived in the very same fashion as for other halide−water interactions.[17] The same Lennard-Jones parameters are used for both ion−water and atom−water interactions for simplicity. Simulations of the photoexcited $NaI(H_2O)$ dynamics performed with a flexible water model,[48] showed that energy transfer to water vibrations in the course of trajectories was negligible, indicating that the rigid water model is adequate for the present simulations. Furthermore, we note that with these model potentials the electronic polarizability of the solvent molecules is kept frozen, instead of being instantaneously equilibrated to the solute charge distribution, in contrast to our earlier solution work.[16] According to high level MRCI ab initio calculations,[49] the water charge distribution does not change significantly between the $NaI(H_2O)$ ground and excited states, such that the static charge distribution of the TIP4P water model is a sensible approximation for small clusters. Overall, we expect our QM/MM potentials to yield reasonably realistic dynamics for this system. As a matter of fact, successful comparison of our simulation results with experiment in section III suggests that this is the case.

B. Molecular Dynamics with Quantum Transitions. Many methods have been developed to simulate non-Born−Oppen-

heimer dynamics.[50−53] In this work, we employ a "surface hopping" trajectory method known as the "molecular dynamics with quantum transitions" (MDQT) method, developed by Tully and co-workers,[54] to follow the dynamics in the excited electronic state and the decay to the ground state. Surface hopping methods are known to describe well nonadiabatic dynamics involving rapid transitions, and we thus believe the MDQT method is best suited for our purpose. In this method, the classical particles (nuclei) are constrained to evolve on an individual adiabatic (electronic) potential energy surface with the quantum (electronic) degrees of freedom propagated simultaneously, and at each trajectory time step, the quantum subsystem time evolution dictates the choice of which adiabatic potential energy surface the dynamics will be propagated on in the following time step.

The time-dependent wave function of the system is expanded in terms of the electronic adiabatic states

$$\Psi(\mathbf{Q},\mathbf{r},t) = \sum_j C_j(t)\, \psi_j(\mathbf{Q},\mathbf{r}) \tag{15}$$

where $\mathbf{Q} = (\mathbf{R},\mathbf{R}^s)$ represents all the nuclear degrees of freedom, i.e., both those of the solute and those of the solvent molecules. The wave function$\Psi(\mathbf{Q},\mathbf{r},t)$is propagated together with the classical nuclear motion, using the "classical path" equations of motion[54]

$$i\hbar\dot{C}_k = \sum_j C_j(V_{kj} - i\hbar\dot{\mathbf{Q}}\cdot\mathbf{d}_{kj}) \tag{16}$$

where

$$V_{kj} = \langle\psi_k|\hat{H}|\psi_j\rangle \tag{17}$$

are the Hamiltonian matrix elements over the adiabatic electronic states and

$$\mathbf{d}_{kj} = \langle\psi_k|\nabla_Q\psi_j\rangle \tag{18}$$

is the nonadiabatic coupling vector between the electronic states, a key ingredient in the equations of motion for the quantum degrees of freedom. In contrast to earlier applications of the MDQT method,[54] where the propagation of the time-dependent wave function relied on a number of numerical approximations, the present mixed semiempirical VB/classical potential representation allows one to compute the elements of the nonadiabatic coupling vector—and thus the right-hand side of the quantum equations of motion, eq 16—analytically, so that the propagation of the quantum degrees of freedom reduces to a two-point boundary value problem, which is solved efficiently and accurately by a second-order finite-difference-equation numerical method.[55]

With the MDQT method, transitions can occur anywhere along trajectories, not just at localized avoided crossings. At each trajectory time step, the probability to undergo a transition is calculated from the time-dependent wave function expansion coefficients as[54]

$$g_{kj} = \frac{f_{jk}\Delta t}{\rho_{kk}} \qquad f_{jk} = 2\hbar^{-1}\,\mathrm{Im}(\rho^*_{jk}V_{jk} - 2\mathrm{Re}(\rho^*_{jk}\mathbf{Q}\cdot\mathbf{d}_{jk})) \tag{19}$$

where Δt is the time step and ρ is the density matrix, i.e., $\rho_{kj} = C_kC_j^*$. A stochastic "fewest switches" algorithm is used to decide whether a hop to another adiabatic state should occur or not.[54] If a switch between states is performed, the energy difference between the states is distributed among the various classical degrees of freedom along the nonadiabatic coupling vector as[54]

$$\dot{\mathbf{Q}}_i' = \dot{\mathbf{Q}}_i - \frac{\gamma_{kk'}\mathbf{d}^i_{kk'}}{m_i} \tag{20}$$

where m_i is the mass of atom i, and

$$\gamma_{kk'} = \frac{b_{kk'} \pm \sqrt{b_{kk'}{}^2 - 4a_{kk'}[V_{kk}(\mathbf{Q}) - V_{k'k'}(\mathbf{Q})]}}{2a_{kk'}}$$

$$a_{kk'} = \frac{\frac{1}{2}\sum_i |\mathbf{d}_{kk'}|^2}{m_i} \qquad b_{kk'} = \sum_i \dot{\mathbf{Q}}_i\cdot\mathbf{d}_{kk'} \tag{21}$$

In the MDQT method, each trajectory is propagated completely coherently; i.e., values of the coefficients of the time-dependent wave function are retained throughout the propagation, and thus, in order to account for quantum decoherence, one needs to propagate a swarm of trajectories for a given single classical initial condition. Each swarm trajectory follows its own path, and the resulting spreading of trajectories leads to a loss of phase coherence when the results are summed over all trajectories.[56] Test calculations showed that a swarm of 100 trajectories was sufficient to obtain converged results for the NaI curve crossing dynamics, and we shall use this swarm size thereafter. Finally, in simulations[57,58] where all or part of the system is described by quantum chemistry/mechanics and the remaining part is described with classical potentials, the "quantum" forces on the nuclei are customarily computed via the Hellmann−Feynman theorem.[59] However, Hellmann−Feynman forces are grossly in error in the small, incomplete basis set representation of semiempirical VB theory employed here, and analytical expressions for the forces with the aforementioned mixed semiempirical VB theory/classical potentials were derived. The nuclear motion is propagated classically with the "velocity" version[60] of the Verlet algorithm,[61] and a stepsize of 0.2 fs, which ensures excellent energy conservation.

C. Simulation of Experimental Data. We apply essentially the same detection schemes as those reported by Jouvet et al. to obtain femtosecond probe signals and photoelectron spectra,[15,24] in which excitation is made to a probe state which asymptotically correlates to $Na^+ + I + e$. Recent ab initio calculations,[62] using Multi-Reference Configuration Interaction with Davidson correction and complete basis set extrapolation (MRCI+Q/CBS), suggest that the $Na^+\cdots I$ complex has two energetically accessible electronic states within the range of experimental probe laser wavelengths employed for the study of bare NaI and $NaI(H_2O)_n$. Spin−orbit coupling of NaI^+ electronic states yields the X ($\Omega = {}^1/_2$) state, with pure Π character, and the I ($\Omega = {}^3/_2$) state, which is a mixture of $^2\Pi$ and $^2\Sigma$ states, as shown in Figure 1. Following selection rules for the photoionization of diatomic molecules proposed by Xie and Zare,[63] transition from the first excited NaI state to both the X and I NaI^+ states are allowed, and promotion to both of these states is considered in our simulations. Accurate analytical potentials for the $^2\Pi$ and $^2\Sigma$ states of the NaI^+ complex have been derived in previous work.[62] The potentials consist of Born−Mayer repulsion terms and London dispersion terms for

TABLE 1: Model Potential Parameters for the $^2\Pi$ and $^2\Sigma$ NaI^+ Probe States of Eq 22

	$^2\Pi$ state	$^2\Sigma$ state
A (kcal/mol)	83340	71547
B ($Å^{-1}$)	2.881	3.064
C [(kcal/mol)/$Å^6$]	7531	3728
α ($Å^3$)	5.02	4.53
Q (e·$Å^2$)	−0.34	0.72

short-range interactions, and ion-induced dipole and ion-quadrupole terms for long-range interactions, i.e.:

$$V_{^2\Pi,^2\Sigma}(R) = Ae^{-Br} - \frac{C}{R^6} - \frac{\alpha e^2}{2R^4} + \frac{Qe}{R^3} \qquad (22)$$

and the parameters, listed in Table 1, were obtained from a standard nonlinear least-squares fit of the MRCI+Q/CBS potential energy curves. A semiempirical approach is used within our simulation procedure to obtain the spin−orbit coupled X- and I-state potential energy curves from the $^2\Pi$- and $^2\Sigma$-state analytical potentials.[62] The resulting X and I states are given by

$$X_{\Omega=3/2}(R) = {}^2\Pi(R) - \lambda \qquad (23)$$

and

$$I_{\Omega=1/2}(R) = \frac{1}{2}\{{}^2\Sigma(R) + {}^2\Pi(R) + \lambda + \sqrt{[{}^2\Pi(R) - {}^2\Sigma(R)]^2 + 2\lambda[{}^2\Pi(R) - {}^2\Sigma(R)] + 9\lambda^2}\} \qquad (24)$$

respectively. The coupling constant λ is calculated from the experimental spin−orbit coupling of the free iodine atom ξ = 7.25 kcal/mol as $\lambda = \xi/2$. Finally, the diabatic probe states are not included when solving for the first two adiabatic states of NaI, as they lie very high in energy and thus do not mix with the ionic and covalent NaI diabatic states.

Two different detection schemes (illustrated in Figure 1) that were employed in previous experimental femtosecond studies of bare NaI and $NaI(H_2O)_n$ clusters have been considered. Because of the dynamic stabilization of the ionic portion of the first NaI excited state by surrounding water molecules, a 2 × 610 nm probe scheme was used for cluster studies,[24] where ionization from the covalent branch of the first excited state was found to be efficient in solvent clusters. For reasons that will become obvious shortly, a second detection scheme was considered in this study, involving a 263 nm probe excitation from the ionic branch of the first excited state, as was used for studies of bare NaI.[15] Essentially, for each excitation−detection (pump−probe) time delay, the species trapped in the first excited-state well, and only those for which the NaI excited state is predominantly covalent, undergo a vertical 2 × 610 nm excitation in the two-photon detection scheme, whereas only those for which the excited state is predominantly ionic undergo a vertical 263 nm excitation in the one-photon detection scheme. If the total energy of the freshly excited species exceeds that of the X and/or I probe state, the species are promoted to the given NaI^+ probe state. As shown in Figure 1, upon promotion to the NaI^+ state, an electron is ejected with a kinetic energy K_{el} corresponding to the excess energy of the ionizing probe photon energy relative to the probe state (while the NaI nuclear kinetic energy remains unaffected by the ejection of the electron). The $Na^+(H_2O)_p$ and the $NaI^+(H_2O)_p$ probe signals, where p represents the detected product cluster size, were evaluated after propagating the $NaI^+(H_2O)_n$ dynamics on the probe state for 4 ps. This time was chosen to account for the long time delay between the probe pulse and detection by time-of-flight mass spectrometry. As done previously,[15] the newly NaI^+ ionized species is considered dissociated if the internal energy exceeds the binding energy of 10.4 and 4.2 kcal/mol for the X state for the I state, respectively.[62] Water molecules are considered evaporated from the NaI excited-state or probe-state complex if their energy exceeds that of the $Na^{(+)}-H_2O$ or $I^{(-)}-H_2O$ binding energies. Finally, the resulting histogram distributions of the $Na^+(H_2O)_p$ and the $NaI^+(H_2O)_p$ species are convoluted with a Gaussian function, with variance of 100−250 fs, to account for the presumably Gaussian experimental pump and probe pulse envelopes.

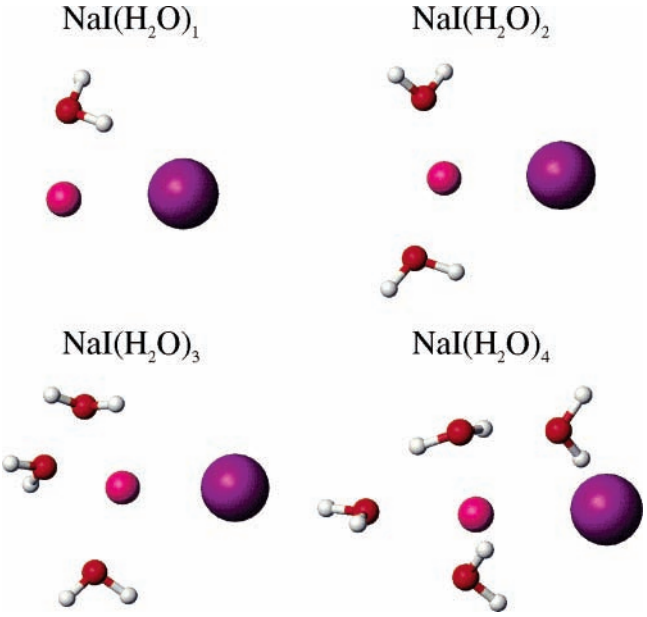

Figure 2. Representative ground-state $NaI(H_2O)_n$ [n = 1−4] cluster structures at 300 K.

III. Results and Discussion

In this section, we first discuss the thermal distributions of $NaI(H_2O)_n$ ground-state structures that serve as initial conditions in the MDQT simulations. The effect of solvation and water evaporation on the simulated excited-state population decay are then discussed. We also examine the water evaporation dynamics and the mechanistic details of the evaporative process, and finally, we connect our simulated probe signals with available experimental data and propose various spectroscopic schemes to further explore the photodissociation dynamics of $NaI(H_2O)_n$ clusters.

A. Ground-State Structures−Initial Conditions. Canonical ensembles of (20n) ground-state $NaI(H_2O)_n$ [n = 1−4] structures, e.g., 60 initial structures for $NaI(H_2O)_3$, were sampled from Nosé molecular dynamics[64] runs performed at 300 K with a modified version of the velocity Verlet algorithm.[65] Because the model potential employs rigid water molecules, there are only six degrees of freedom per water molecule, and thus 20 initial conditions per water molecule represents adequate sampling. Representative structures for each cluster size are shown in Figure 2, and the distributions of $Na-H_2O$ intermolecular distances $P(R_{Na-H_2O})$ as a function of cluster size are displayed in Figure 3. Because the room-temperature binding energy of Na^+ to water (24 kcal/mol) is much higher than that of I^- to water (∼10 kcal/mol),[66−68] the water molecules will tend to bind to the sodium end of NaI in the ground ionic state,

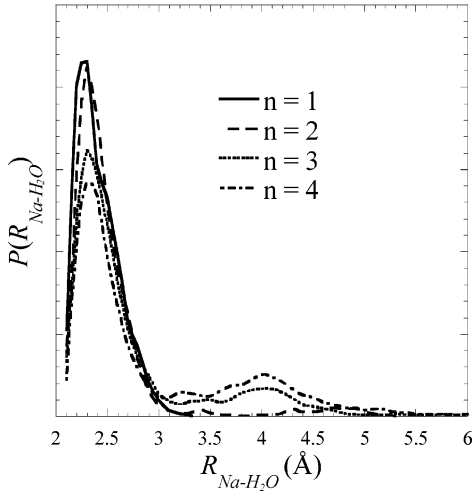

Figure 3. Thermal distribution of initial Na−H_2O distances $P(R_{Na-H_2O})$ obtained from Nosé molecular dynamics simulations of ground-state $NaI(H_2O)_n$ clusters of size 1 (solid), 2 (dash), 3 (dot) and 4 (dash−dot).

as illustrated in Figure 2. For all cluster sizes, a peak in the R_{Na-H_2O} distribution, shown in Figure 3, occurs at ca. 2.3 Å, which is approximately the equilibrium Na^+-H_2O distance predicted by ab initio calculations for small $Na^+(H_2O)_n$ clusters.[25] For larger $NaI(H_2O)_n$ [$n = 3, 4$] clusters, a broad, second peak centered at $R_{Na-H_2O} \sim 4.0$ Å appears in the distributions. This broad peak corresponds to ∼2% of the whole population of water molecules, which transiently dwell on the iodide end of ground-state NaI.

The canonical ensembles of configurations provide initial cluster structures for the MDQT simulations. In contrast to our previous $NaI(H_2O)$ photodissociation dynamics study where a 296 nm pump pulse was used,[17] $NaI(H_2O)_n$ clusters undergo a simple vertical Franck−Condon excitation with an energy corresponding to the difference between the ground and first excited-state potential energies ΔE_{FC}. Due to thermal excitation and the dynamically changing solvent environment, the ground-state NaI internuclear distance R varies significantly with cluster size, as evidenced by the distributions $P(R)$ shown in Figure 4a. Accordingly, the initial FC excitation energy differs for each starting $NaI(H_2O)_n$ cluster configuration, resulting in FC energy gap distributions, which are shown in Figure 4b. The average ΔE_{FC}, listed in Table 2, increases as a function of cluster size, which results in an overall increase of 2.3 eV for $NaI(H_2O)_4$, compared to that of bare NaI. The recent pump−probe experiment of Grégoire et al. suggests that the maximum in the absorption efficiency as a function of laser wavelength for $NaI(H_2O)_2$ is blue-shifted by 1.1 eV relative to that of bare NaI, and by 1.3 eV for $NaI(H_2O)_{16}$.[24] Ab initio MRCI calculations using a double-ζ basis set predict excitation energies for $NaI(H_2O)_2$ and $NaI(H_2O)_4$ 1.1 and 1.2 eV larger than for bare NaI, respectively,[49] in good agreement with experimental findings. Due to the discrepancy between our simulated ΔE_{FC} and the experimental and ab initio results, we limit our simulations to small cluster sizes where the discrepancy in FC energy gap is not too large. As will be discussed later, this discrepancy is not a major concern and is of no consequence for the actual excited-state dynamics.

B. Nonadiabatic Dynamics. The excited-state population lifetimes resulting from the MDQT simulations are displayed in Figure 5. For all cluster sizes, a sharp initial drop in the excited-state population occurs at ca. 200 fs, which roughly corresponds to the time at which the NaI system reaches the

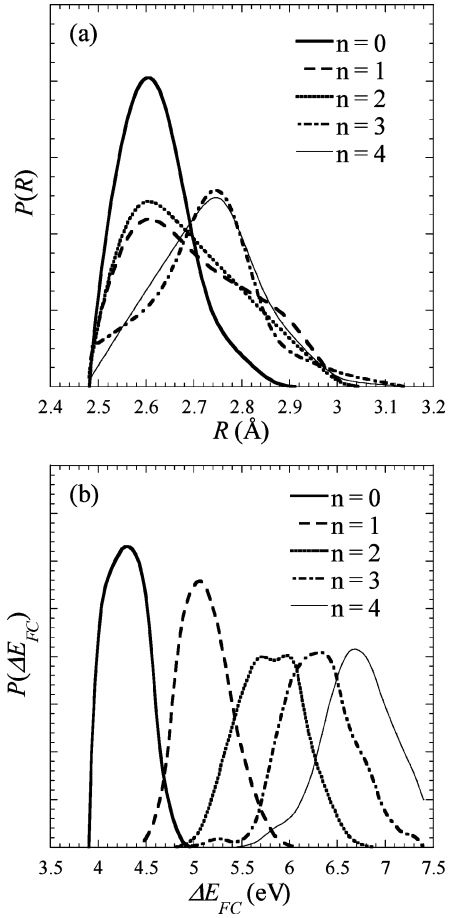

Figure 4. Distributions of (a) ground-state NaI internuclear separations $P(R)$, and (b) ground-to-excited-state Franck−Condon (FC) energy gaps $P(\Delta E_{FC})$, for $NaI(H_2O)_n$ clusters of size 0 (solid), 1 (dash), 2 (dot), 3 (dash−dot) and 4 (thin solid). Data have been smoothed to remove slight numerical noise.

crossing region for the first time t_c, as supported by the average times at which NaI reaches the diabatic curve-crossing point for the first time $\langle t_c \rangle$ listed in Table 2. The drop in the excited-state population in the crossing region increases as a function of cluster size because the outer ionic portion of the excited-state curve is increasingly stabilized by the presence of water molecules. This is illustrated by the NaI−H_2O Coulombic interaction energies in the ionic state $\langle V^C_{1,1c} \rangle$ in the curve-crossing region, listed in Table 2, which increases in magnitude with cluster size. As a result, the average covalent/ionic curve-crossing points $\langle R_c \rangle$, also listed in Table 2, increases with cluster size, and because the NaI electronic coupling decreases exponentially with increasing internuclear distance, the excited- to ground-state transition probability increases with cluster size, and the excited-state population decay also increases. Moreover, the excited-state population decay is enhanced by dynamical fluctuations in the relative position of the diabatic covalent and ionic states caused by the motion of the surrounding water molecules, which sometimes results in multiple nonadiabatic transitions during the first NaI oscillation period.

As was found previously for $NaI(H_2O)$,[17] the $NaI(H_2O)_n$ [$n = 1-4$] excited-state population decay resembles that of bare NaI after reaching the curve-crossing region for the first time ($t > 200$ fs), as can be seen from Figure 5. As will be discussed in more detail in the following section, the initial repulsive force arising from the reversed NaI polarity causes the evaporation of 99% of the water molecules for $NaI(H_2O)$ and 95% for $NaI(H_2O)_n$ [$n = 2-4$] by the time the NaI system reaches the curve-

TABLE 2: $NaI(H_2O)_n$ Properties[a]

n	0	1	2	3	4
$\langle \Delta E_{FC} \rangle$ (eV)	4.2 ± 0.1	5.0 ± 0.2	5.7 ± 0.3	6.2 ± 0.3	6.7 ± 0.4
$\langle t_c \rangle$ (fs)	156 ± 10	168 ± 22	178 ± 22	182 ± 33	183 ± 40
$\langle V^C_{11,c} \rangle$ (kcal/mol)		-1 ± 2	-3 ± 4	-4 ± 4	-5 ± 4
$\langle R_c \rangle$ (Å)	6.6 ± 1.3	7.1 ± 1.3	7.7 ± 1.3	8.1 ± 1.3	8.3 ± 1.3
$\langle T \rangle$ (fs)	1600 ± 300	1400 ± 400	1300 ± 500	1200 ± 700	1200 ± 800
$\langle F^0_{Na-O} \rangle$ [(amu·Å)/fs^2]		24 ± 15	10 ± 10	16 ± 10	9 ± 8
$\langle \tau^0 \rangle$ (amu/fs^2)		14 ± 3	15 ± 3	16 ± 4	16 ± 4
$\langle E^0_{FC} \rangle$ (kcal/mol)	30 ± 2	37 ± 5	46 ± 6	52 ± 7	56 ± 8

[a] Average properties over ensembles of configurations, along with standard deviations. ΔE_{FC} is the Franck−Condon energy gap, t_c is the time at which NaI reaches the curve-crossing region for the first time, $V^C_{11,c}$ is the Coulombic interaction energy between the water molecule and ionic NaI at the curve-crossing point, R_c is the NaI internuclear separation at the curve-crossing point, T is the NaI vibrational period on the first excited state, F^0_{Na-O} is the magnitude of the force acting on the water oxygen atom due to sodium upon excitation, τ^0 is the magnitude of the torque induced on the water molecule by NaI upon excitation, and E^0_{FC} is the excess Franck−Condon energy upon excitation.

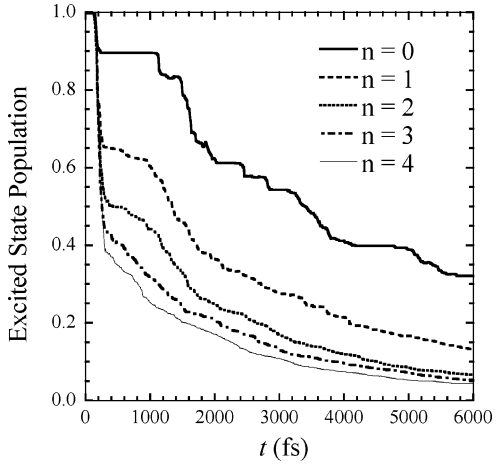

Figure 5. Excited-state population as a function of simulation time obtained from MDQT simulations of $NaI(H_2O)_n$ clusters of size 0 (solid), 1 (dash), 2 (dot), 3 (dash−dot) or 4 (thin solid).

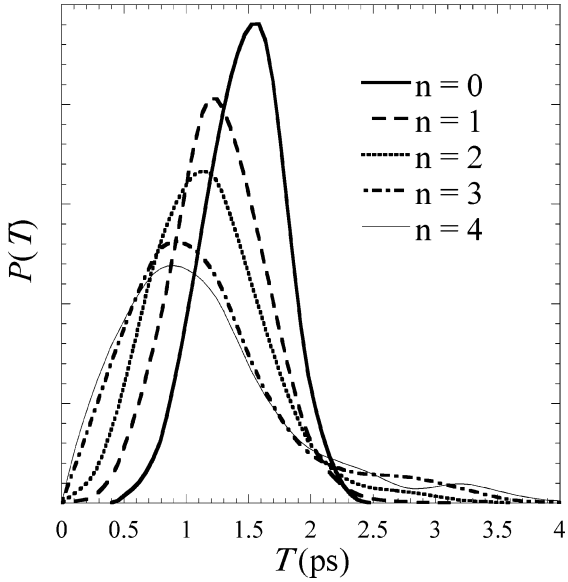

Figure 6. Distributions of excited-state NaI vibrational periods $P(T)$ for $NaI(H_2O)_n$ clusters of size 0 (solid), 1 (dash), 2 (dot), 3 (dash−dot) and 4 (thin solid). The vibrational periods were evaluated over clusters that remain in the excited state. Data have been smoothed to remove slight numerical noise.

crossing region for the first time, the water evaporation time t_{evap} being defined as the time at the last inner turning point in the Na−H_2O or I−H_2O bound motion. Nonetheless, the evaporated water molecules are at an average distance of only 5 ± 2 Å from NaI when it reaches the curve-crossing region for the first time (the average distance, which exhibits very little cluster size dependence, is evaluated over all configurations and cluster sizes). The water molecules are therefore still close enough to NaI to affect the excited-state dynamics in the crossing region, but solvation effects decline rapidly as the water molecules move further away from the solute, such that the $NaI(H_2O)_n$ long-time excited-state dynamics are not significantly affected by the presence of water, and consequently resemble that of bare NaI.

The periodic features in the long-time excited-state decay observed for bare NaI disappear with increasing cluster size. Some periodicity in the excited-state population decay for the first NaI oscillation period is still apparent for cluster sizes 1 and 2, but it disappears completely for larger cluster sizes. The distributions of excited-state NaI vibrational periods $P(T)$ for the trajectories that remain in the excited state after reaching the curve-crossing region for the first time are shown in Figure 6. The disappearance of the periodicity in the NaI vibrational motion with increasing cluster size is due to vibrational dephasing, as evidenced by the broadening of the $P(T)$ distributions with cluster size. Furthermore, the positions of the distribution peaks, and the corresponding average vibrational periods $\langle T \rangle$, listed in Table 2, decrease with cluster size, suggesting that NaI has increasingly less post-H_2O evaporation residual energy. We also note that, in the cluster case, the vibrational period can extend beyond that of gas-phase NaI, due to solvation of the ionic portion of the excited state when water remains bound to either the Na or I end of NaI after reaching the nonadiabatic transition region, as evidenced by the long tail in the $P(T)$ distributions for cluster sizes 2 to 4, shown in Figure 6.

As seen in Figure 5, the increased NaI nonadiabatic transition probability caused by the presence of surrounding solvent molecules results in a reduction of 18% to 28%, depending on cluster size, in the number of trajectories where NaI remains bound in the excited state over the simulation time scale, relative to bare NaI. For instance, 92% of the $NaI(H_2O)_4$ trajectories lead to dissociated ground-state atoms and 5% of the NaI population remains bound in the excited state after 6 ps, compared to 68% and 32%, respectively, for bare NaI. Interestingly, transitions to the ionic branch of the ground state occur during the simulation time scale for 3% of the $NaI(H_2O)_4$ population due to NaI−H_2O energy transfer upon and prior to water evaporation, as will be discussed in more detail later.

C. Water Evaporation Dynamics. As mentioned in the previous section, the long-time excited-state $NaI(H_2O)_n$ [$n = 1-4$] populations, i.e., for $t > 200$ fs, are similar to that of

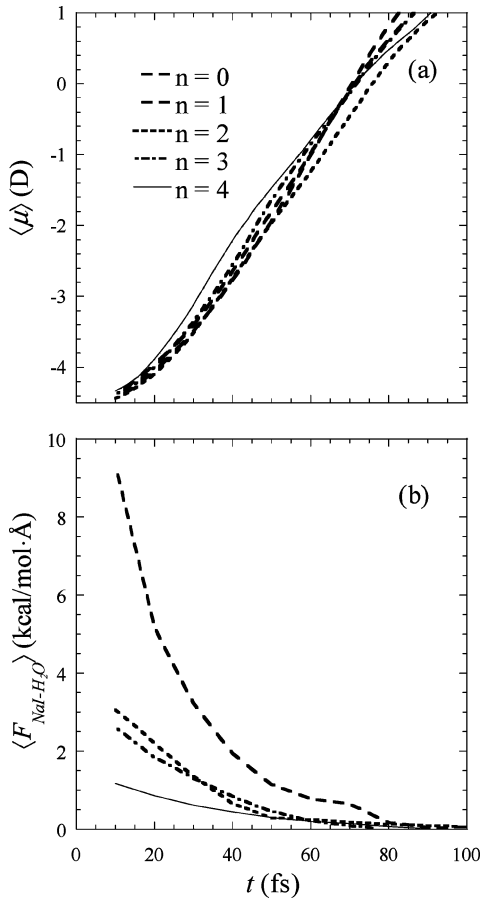

Figure 7. (a) Average NaI dipole moment $\langle\mu\rangle$ and (b) average force exerted by NaI on H_2O $\langle F_{NaI-H_2O}\rangle$ as a function of simulation time for $NaI(H_2O)_n$ clusters of size 0 (solid), 1 (dash), 2 (dot), 3 (dash−dot) and 4 (thin solid).

bare NaI due to rapid water evaporation after vertical excitation to the first excited state. In our previous $NaI(H_2O)$ photodissociation dynamics study,[17] rapid water evaporation was found to be caused mainly by the reversed polarity of NaI in the Franck−Condon region of the first excited state. The average NaI dipole moment $\langle\mu\rangle$ and the average magnitude of the force exerted by NaI on the surrounding water molecules $\langle F_{NaI-H_2O}\rangle$ as a function of time and cluster size are displayed in Figure 7. After approximately 100 fs, the average NaI−H_2O repulsive force vanishes for all cluster sizes. Thus, water evaporation occurring before 100 fs is caused exclusively by the NaI−H_2O repulsive interactions induced by excitation of NaI to the predominantly covalent portion of the adiabatic excited state. Furthermore, the fact that most water molecules evaporate within 100 fs of excitation, where the evaporation time is defined as the time of the last turning point in the Na−H_2O or I−H_2O bound motion, suggests an extremely nonstatistical evaporation process, because internal vibrational energy redistribution is unlikely to occur on such a short time scale.

To validate the present findings and the assumptions inherent in our QM/MM model, we compare the NaI−H_2O excited-state forces, after vertical excitation from the ground-state minimum energy structure, with those obtained from MRCI/DZ calculations.[49] As mentioned previously, NaI has a reversed polarity in the Franck−Condon region of the excited state, leading to repulsive NaI−H_2O forces. As a result, the negatively charged sodium atom will initially repel the oxygen atom, and thus the water molecule, and then it will attract the lighter hydrogen atoms, inducing a torque on the water molecule. In Table 3,

TABLE 3: Properties of the Excited-State NaI−H_2O Forces[a]

	QM/MM	MRCI/DZ
$F^0_{NaI-H_2O}$ [(kcal/mol)·Å]	14.8	14.2
θ^0 (deg)	90	90
τ^0 (kcal/mol)	14.3	18.2

[a] Obtained from mixed semiempirical/classical potentials (QM/MM) and from high level ab initio (MRCI/DZ) calculations [cf. ref 49] for the minimum energy ground-state structure. $F^0_{NaI-H_2O}$ is the magnitude of the force exerted on the water center of mass by NaI, θ^0 is the angle between the NaI internuclear coordinate and the NaI−H_2O force, and τ^0 is the magnitude of the torque exerted on the water molecule.

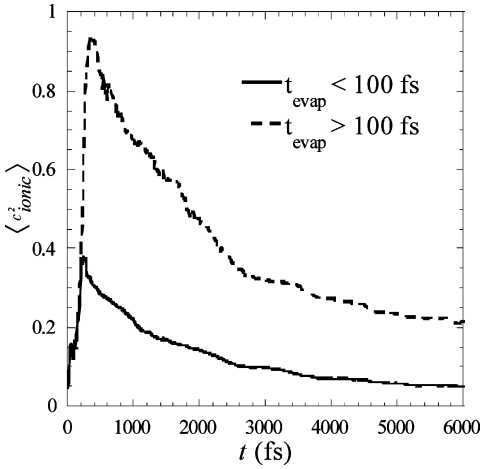

Figure 8. Average weight of the ionic state in the NaI electronic structure $\langle c^2_{ionic}\rangle$ as a function of simulation time for short-lived ($t_{evap} \leq 100$ fs) and long-lived ($t_{evap} > 100$ fs) $NaI(H_2O)_n$ clusters [$n = 1-4$]. The ensemble average is evaluated over the full population of short-lived or long-lived clusters, regardless of parent cluster size.

we list the magnitude of the NaI repulsive force acting on the center of mass of the water F_{NaI-H_2O}, the angle between the NaI internuclear coordinate and the NaI−H_2O force θ, and the torque induced on the water τ in the excited state. Both the magnitude and the direction of the NaI−H_2O force obtained with the QM/MM potentials agree very well with the MRCI/DZ results. The QM/MM torque induced on the water molecule is also in relatively good agreement with its ab initio counterpart, with a difference of 21%. We can therefore assume that the forces acting on the water molecules upon photoexcitation to the first NaI excited state yield relatively realistic water evaporation dynamics.

As the system approaches the curve-crossing region, the NaI ionic character increases, and as such the average NaI dipole moment (cf. Figure 7a) of the nascent NaI and the NaI−H_2O binding energy increase sharply (the binding energy of water to ionic NaI is 20 kcal/mol, whereas that to covalent is less than 1 kcal/mol, according to our QM/MM potentials). Therefore, if NaI remains in the excited state after reaching the curve-crossing region, water molecules that lie near the sodium or the iodine end of NaI may become transiently or permanently bound. The average NaI ionic character $\langle c^2_{ionic}\rangle$ is shown in Figure 8 as a function of simulation time for both short-lived and long-lived $NaI(H_2O)_n$ clusters. As might be expected, the ionic character of the long-lived clusters is much larger than that of short-lived clusters on the simulation time scale, thus supporting the fact that water molecules tend to stay bound to NaI with a predominantly ionic electronic structure. Furthermore, these relatively rare events occur when the excess Franck−Condon energy in the NaI internuclear coordinate, gained from pump excitation, is small to start with (averages

TABLE 4: Product Energy Distributions from $NaI(H_2O)_n$ Photodissociation[a]

n		1	2	3	4
$t_{evap} \leq 100$ fs	$\langle E_{trans}(H_2O)\rangle$	6 ± 4	4 ± 2	4 ± 3	3 ± 3
	$\langle E_{rot}(H_2O)\rangle$	9 ± 4	10 ± 5	8 ± 5	7 ± 6
	$\langle E_{total}(NaI)\rangle$	19 ± 9	19 ± 8	16 ± 9	15 ± 8
$t_{evap} > 100$ fs	$\langle E_{trans}(H_2O\rangle$		5 ± 6	6 ± 7	4 ± 6
	$\langle E_{rot}(H_2O)\rangle$		11 ± 8	8 ± 8	7 ± 7
	$\langle E_{total}(NaI)\rangle$		15 ± 10	11 ± 10	13 ± 9

[a] Average translational $\langle E_{trans}(H_2O)\rangle$, rotational $\langle E_{rot}(H_2O)\rangle$, and total NaI $\langle E_{total}(NaI)\rangle$ energies, in kcal/mol, along with standard deviations, for short-lived clusters ($t_{evap} \leq 100$ fs), and long-lived clusters ($t_{evap} > 100$ fs).

listed in Table 2), or has already been depleted by the evaporation of neighboring water molecules, resulting in a smaller NaI vibrational period and slower NaI relative motion.

D. NaI−H_2O Energy Transfer and Mechanistic Aspects. As discussed in the previous section, 99% of the water molecules for $NaI(H_2O)$ and 95% for $NaI(H_2O)_n$ [$n = 2-4$] evaporate on a short time scale due to highly repulsive NaI−H_2O forces that arise from the reversed NaI polarity in the Franck−Condon region of the excited state. Upon excitation, the oxygen atom is repelled by the partial negative charge on the sodium atom, as evidenced by the average magnitude of the force exerted by $Na^{-\delta}$ on the water oxygen atom $\langle F^0_{Na-O}\rangle$ upon excitation, and the post-evaporation average water translational energy $\langle E_{trans}(H_2O)\rangle$ (relative to the NaI center of mass) for short-lived clusters ($t_{evap} \leq 100$ fs), listed in Tables 2 and 4, respectively. Furthermore, the water hydrogen atoms are attracted toward the $Na^{-\delta}$, and due to the light mass of the hydrogen atoms, considerable torque is induced on the water upon excitation, as shown of the average magnitude of the torque $\langle \tau^0\rangle$ in Table 2, resulting in significant rotational excitation. As found previously for $NaI(H_2O)$,[17] the average water rotational energies are greater than the average translational energies for all cluster sizes, especially for short-lived clusters. The strong repulsive forces exerted on the water molecules upon NaI excitation thus induce nonstatistical evaporation, and result in water molecules that are more rotationally hot than translationally hot.

For comparison, simulations of NaI excitation to the purely covalent (and repulsive) $\Omega = 1$ state, rather than to the $\Omega = 0^+$ state, were performed. As expected, 100% of the water molecules evaporate within 100 fs following NaI excitation to the $\Omega = 1$ state. Furthermore, the energy partitioning of the evaporated products for $NaI(H_2O)_n$ is the same for the $\Omega = 1$

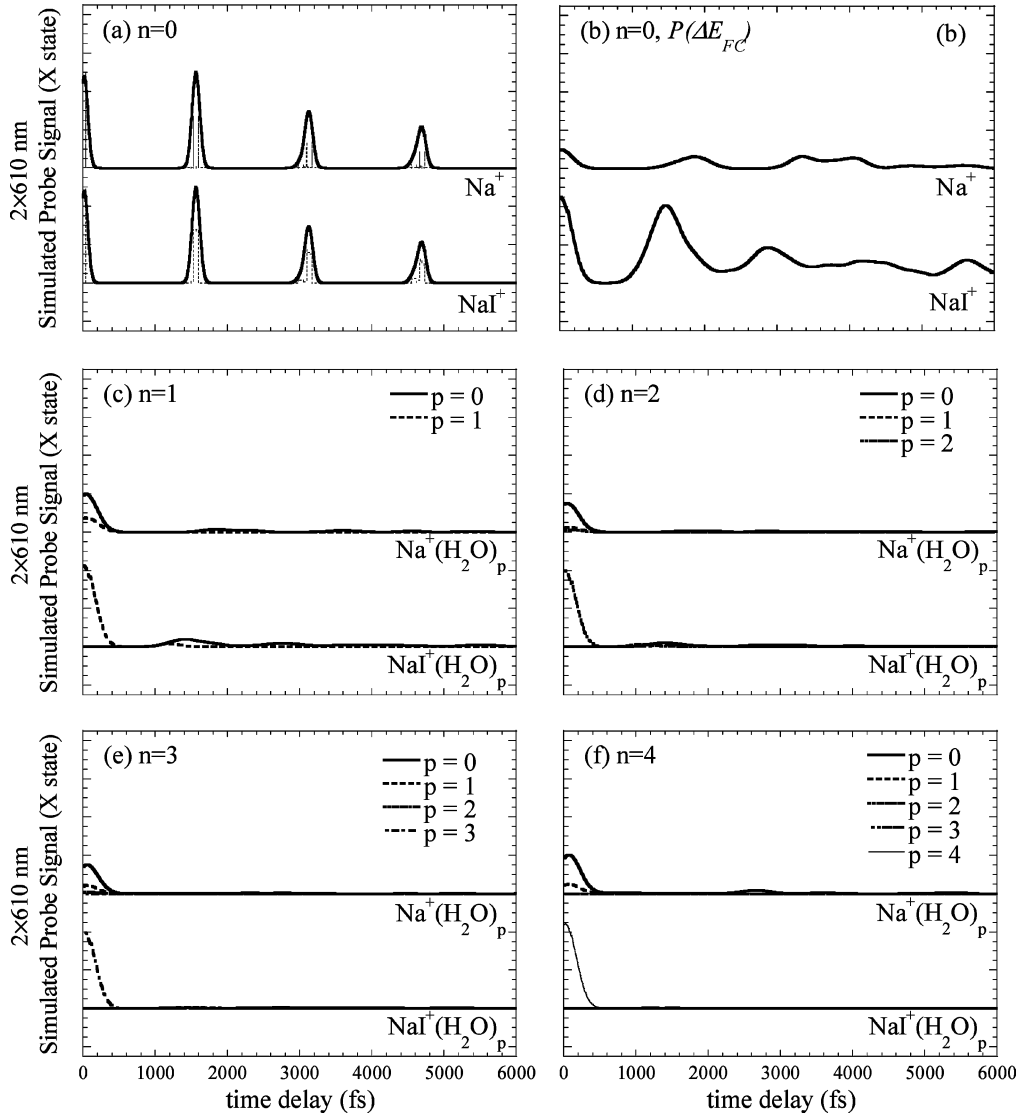

Figure 9. Probe signals for $NaI(H_2O)_n$ photodissociation as a function of pump−probe time delay, generated using a 2×610 nm excitation from the covalent branch of the NaI first excited state to the X probe state. The product cluster size p is 0 (solid), 1 (dash), 2 (dot), 3 (dash−dot) and 4 (thin solid).

state as that for the short-lived clusters excited to the $\Omega = 0^+$ state. In $NaI(H_2O)_4$ clusters, for instance, 3 ± 3 kcal/mol is transferred to water relative translational energy and 7 ± 5 kcal/mol in rotational energy for excitation to the $\Omega = 1$ state. Therefore, the translational and rotational $NaI-H_2O$ energy transfer mechanisms in short-lived clusters excited to the $\Omega = 0^+$ state is entirely governed by the initial repulsive dynamics and is not influenced whatsoever by curve-crossing dynamics.

We previously mentioned that 5% of the water molecules for $NaI(H_2O)_n$ clusters [$n = 2-4$] remain transiently or permanently bound mainly to the sodium end of NaI due to changes in the NaI electronic structure. From Table 4, NaI obviously has less average internal energy $\langle E_{int}(NaI)\rangle$ in long-lived clusters than in short-lived clusters and the average translational energy of the evaporated water molecules is slightly larger for long-lived clusters. Therefore, when water molecules remain bound, NaI primarily transfers energy to water translational motion, whereas the water molecules seem to retain the rotational energy gained due to the initial repulsive dynamics, resulting in a lower total average NaI internal energy for long-lived clusters.

E. Connection with Experiment. In this section, we explore various spectroscopic schemes to probe the NaI photodissociation dynamics in water clusters. As mentioned earlier, the photodissociation dynamics of NaI in water clusters has been previously studied by femtosecond pump−probe spectroscopy employing a 2×610 nm detection scheme, where photoexcitation to the probe state occurs from the covalent branch of the excited state.[24] For an initial cluster size distribution between 1 and 7 water molecules, exponentially decaying $Na^+(H_2O)_p$ experimental probe signals, where p refers to the product cluster size post-water evaporation, were obtained with $p = 1-3$, and $NaI^+(H_2O)_p$ signals were presumably not detected. Our simulation results using the same two-photon detection scheme are shown in Figures 9 and 10 for photoexcitation to the X and I probe states, respectively. To the best of our knowledge, experimental probe signals for bare NaI have not been reported. The simulated probe signals for bare NaI resulting from excitation of NaI at its ground-state equilibrium distance of 2.7 Å are shown in Figures 9a and 10a, whereas those resulting from excitation of NaI with a distribution of room-temperature ground-state internuclear distances $P(R)$ (cf. Figure 4a) are shown in Figures 9b and 10b. Our results suggest that the I state is not energetically accessible with the two-photon probe scheme, and excitation occurs mainly to the NaI^+ potential energy well of the X state. The NaI^+ signal in Figure 9a is oscillatory, reflecting the NaI transient trapping in the excited-state well, normally peaking at the inner turning point of the vibrational motion, and the signal decays over time due to nonadiabatic transitions to the ground state. The signal is broader in Figure 9b and seems to decay more rapidly due to vibrational dephasing caused by the initial ground-state distribution of NaI internuclear distances.

The simulated $Na^+(H_2O)_p$ and $NaI^+(H_2O)_p$ signals as a function of pump−probe time delay are also shown in Figure 9 for excitation to the X state, and Figure 10 for excitation to the I state. Conversely to experimental results, exponentially decaying $NaI^+(H_2O)_p$ signals that are more intense than the $Na^+(H_2O)_p$ signals are detected for excitation to both probe states. The simulated probe signals for bare NaI suggested that the two-photon probe pulse promotes the excited-state complex mainly to the potential energy well of the X state. It is therefore not surprising to obtain $NaI^+(H_2O)_p$ signals that are more intense than the $Na^+(H_2O)_p$ signals. Furthermore, the NaI^+ probe states are stabilized by the presence of surrounding water molecules, relative to the covalent branch of the excited state, such that the I state becomes energetically accessible. In fact, the stabilization energy of the probe states ranges from 18 to 50 kcal/mol for $n = 1-4$. Because photoionization occurs from the covalent branch of the excited state, the signals resulting from the two-photon probe scheme at short pump−probe time delays correspond to a multiphoton vertical excitation directly from the ground state to either the X or the I probe state. In the ground state, the waters are mainly located on the Na end of NaI (cf. Figures 2 and 3). Therefore, upon rapid excitation to a given probe state, the water molecules, which have not moved more than 5 Å away from the NaI on the excited state, are attracted to the Na^+ end of NaI^+ very much like in the ground state, resulting in $NaI^+(H_2O)_p$ signals that correspond to the parent cluster size. On the other hand, $Na^+(H_2O)_p$ signals are only obtained for $p = 0$ and 1 for parent cluster sizes 1−4. The $Na^+(H_2O)_p$ signals arise mainly when excitation occurs to the repulsive wall of the X or I probe states. Because the probe states are stabilized by the presence of water molecules, excitation occurs higher on the probe-state repulsive wall than for bare NaI, and NaI therefore rapidly gains a large amount of kinetic energy after departing from the wall. The excess energy is also released through evaporation of water molecules on the probe state, and thus, a strong bare Na^+ probe signal with a residual $Na^+(H_2O)_4$ [$p = 1$] signal is observed. Finally, in agreement with experimental findings,[24] the probe signals decay exponentially over the first NaI excited-state vibrational period with very little evidence of long-time dynamics. In conclusion, the simulated probe signals obtained with the two-photon probe scheme are not revealing of the NaI photodissociation dynamics beyond the time NaI reaches the curve-crossing region for the first time and therefore do not provide valuable information on the influence of water molecules on the NaI excited-state dynamics. However, our simulations suggest that the parent cluster size can be inferred from the $NaI^+(H_2O)_p$ signals, an issue that may deserve further experimental investigation.

We now turn our attention to the simulated probe signals resulting from the one-photon detection scheme, where probe excitation occurs from the ionic branch of the excited state, and which are displayed in Figures 11 and 12 for excitation to the X and I states, respectively. For bare NaI, in agreement with experimental findings,[6,15] we obtain a broad oscillatory Na^+ signal, reflecting the NaI transient trapping in the excited-state well, that decays with increasing pump−probe time delay due to nonadiabatic transitions, as shown in panels a and b of Figures 11 and 12. For excitation to the X state, the Na^+ signal decreases as the NaI^+ signal increases as the latter arises from excitation at the outer turning point in the excited-state NaI vibrational motion.[6,15] At the outer turning point, NaI has very little or no kinetic energy, and because the X state is still slightly binding at this internuclear distance because of long-range interactions,[62] NaI will not have enough residual kinetic energy after promotion to the X state to allow for dissociation of the NaI^+ complex. Consequently, we obtain a narrow NaI^+ signal, which spans ~30 fs, as evidenced by the unconvoluted probe signals shown in Figure 11a, and a corresponding decrease in the Na^+ signal at the outer turning point in the NaI excited-state vibrational motion. As shown in Figure 12a, excitation to the I state, however, does not produce a NaI^+ signal because of a small barrier of ~0.1 kcal/mol in the I state at an internuclear distance of ~5 Å (the barrier is barely perceptible in Figure 1), which prevents NaI^+ complex formation, because of excitation to the product side of the barrier, with very little nuclear kinetic

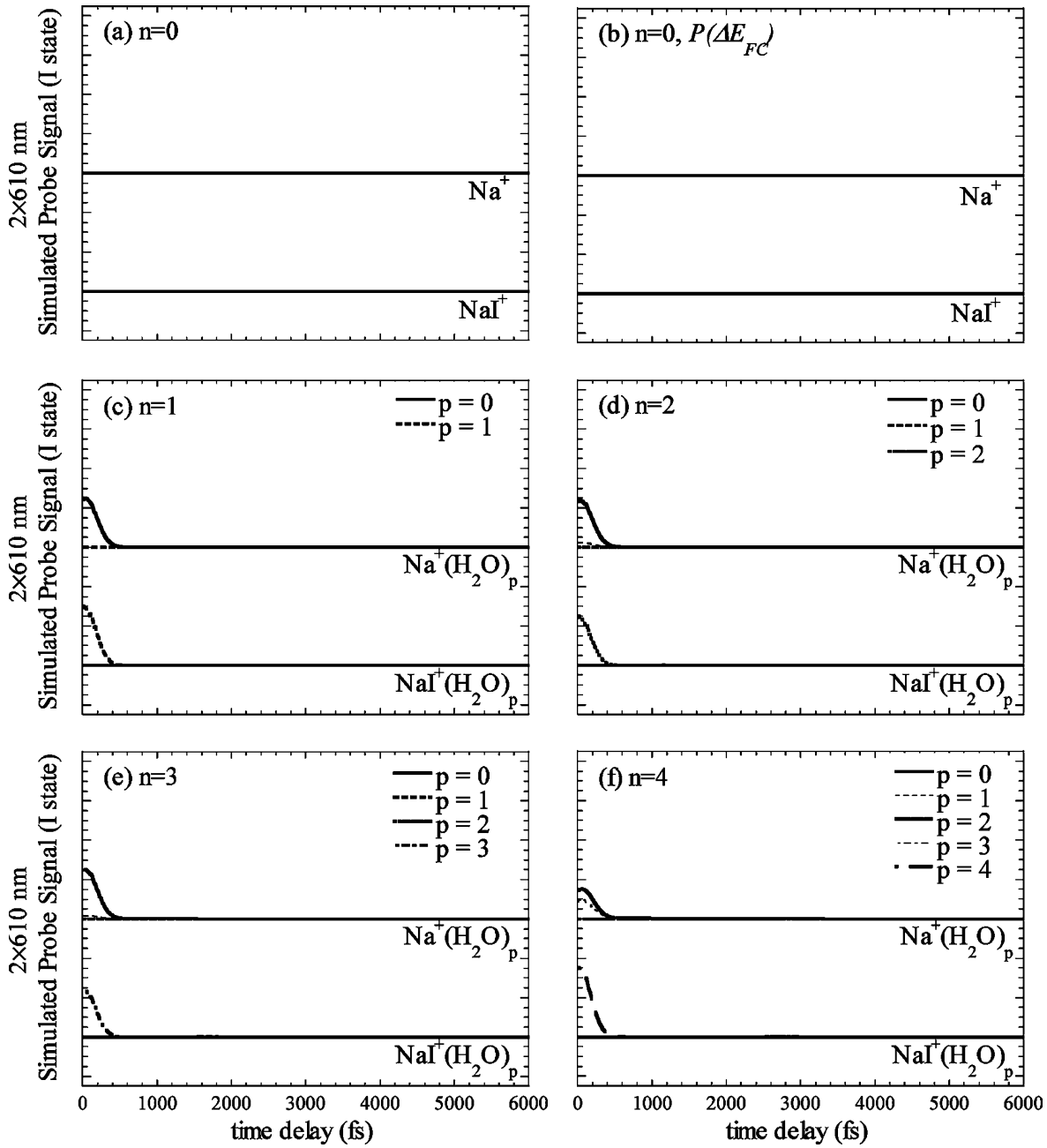

Figure 10. Probe signals for NaI$(H_2O)_n$ photodissociation as a function of pump−probe time delay, generated using 2 × 610 nm excitation from the covalent branch of the NaI first excited state to the I probe state. The product cluster size p is 0 (solid), 1 (dash), 2 (dot), 3 (dash−dot) and 4 (thin solid).

energy.[62] Once again, the probe signals obtained for photoionization of NaI with a distribution of room-temperature ground-state internuclear distances are broader and the oscillatory features due to NaI transient trapping in the excited-state well are damped because of vibrational dephasing.

The simulated $Na^+(H_2O)_p$ and $NaI^+(H_2O)_p$ probe signals obtained from the one-photon probe scheme are also shown in Figures 11 and 12 for photoexcitation to the X and I states, respectively. Bare Na^+ signals that decay with increasing pump−probe time delay due to nonadiabatic transition are detected, and $Na^+(H_2O)_p$ signals are not observed due to further water evaporation on the probe state caused by excitation to the repulsive wall of the probe state, very much like in the two-photon probe situation. The signals are very similar for excitation to the X and I probe states, with an intensity that decreases slightly as a function of cluster size, reflecting the increase in the excited-state population decay (cf. Figure 5) when NaI reaches the curve-crossing region for the first time, as mentioned earlier. On the other hand, faint $NaI^+(H_2O)_p$ signals are detected for excitation to the X state, and not to the I state due to the small barrier at ∼5 Å mentioned earlier. The first peak corresponds to the parent cluster size, because the water molecules do not move far enough from NaI prior to promotion to the X state, as was the case for the $NaI^+(H_2O)_p$ probe signals resulting from the two-photon probe scheme. The successive evaporation of water molecules at longer pump−probe time delays can also be observed from the $NaI^+(H_2O)_p$ signals. We can conclude that the probe signals resulting from the one-photon detection scheme show evidence of increased nonadiabatic transitions due to the stabilization of the ionic branch of the excited state. Moreover, the successive evaporation of water molecules due to the repulsive dynamics in the covalent region

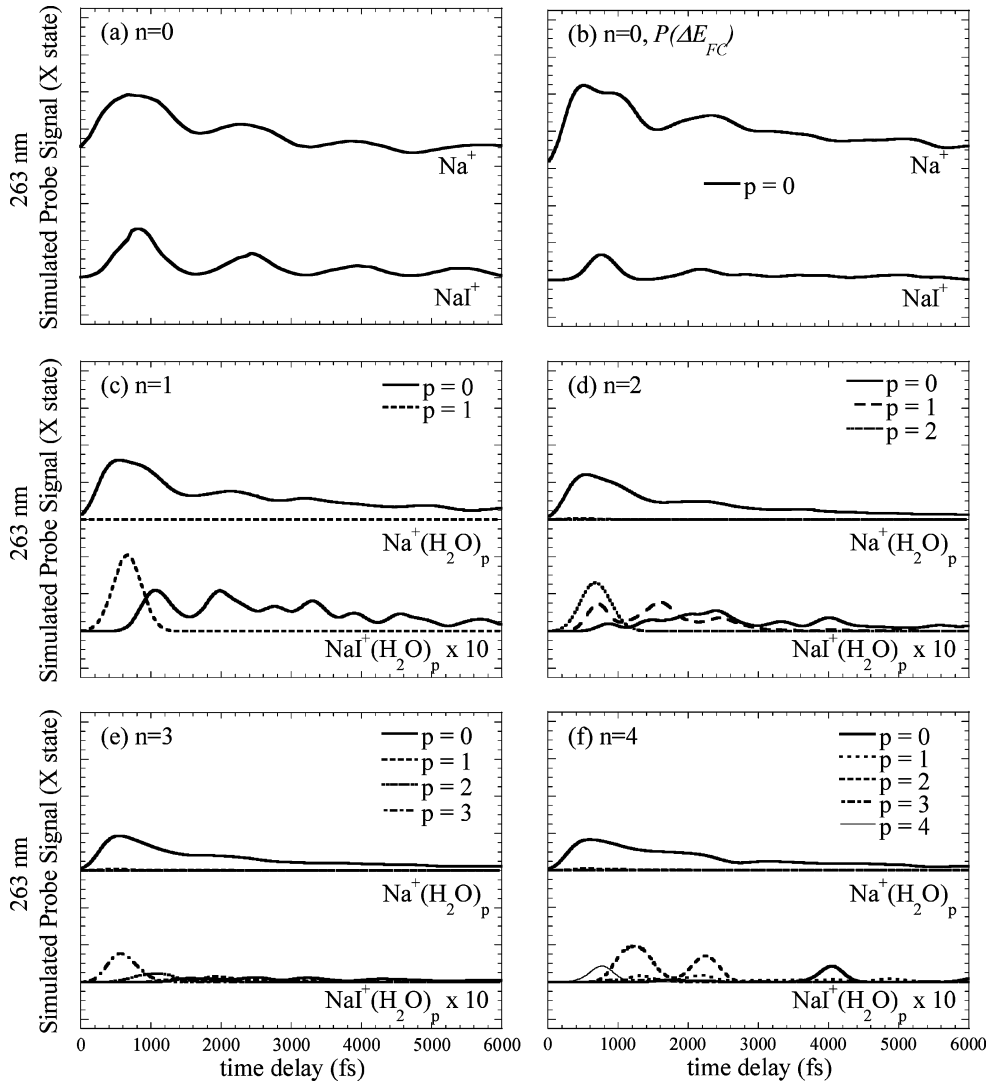

Figure 11. Probe signals for $NaI(H_2O)_n$ photodissociation as a function of pump−probe time delay, generated using a 263 nm excitation from the ionic branch of the NaI first excited state to the X probe state. The product cluster size p is 0 (solid), 1 (dash), 2 (dot), 3 (dash−dot) and 4 (thin solid). The $NaI^+(H_2O)_p$ probe signals have been magnified by a factor of 10 relative to the $Na^+(H_2O)_p$ signals due to the low intensity of the signals.

of the excited state can be monitored from the $NaI^+(H_2O)_p$ probe signals, given that the signals are sufficiently intense to be detected experimentally. The probe signals resulting from the one-photon probe scheme are thus much more revealing of the influence of water molecules on NaI photodissociation dynamics. Even though the two-photon probe scheme could be expected to be less sensitive to solvation because excitation occurs from the covalent branch of the NaI first excited state, our simulation results reveal that the one-photon scheme is even less sensitive to solvation in small clusters because the water molecules are bound mainly to the Na^+ end of NaI on both the ionic branch of the excited state and the probe state, such that both states are stabilized to the same extent by the presence of water molecules. On the other hand, excitation energies from the covalent branch of the first excited state, as in the two-photon probe scheme, depend on the solvation of the sodium ion on the probe state.

Time-resolved photoelectron spectra obtained with the one-photon probe scheme are shown in Figure 13. The photoelectron spectra obtained with the two-photon probe scheme are not shown because very little information beyond the time at which NaI reaches the curve-crossing region for the first time can be inferred from the spectra. Furthermore, the spectra for excitation to the I state are not shown because they are very similar to those for excitation to the X state. For bare NaI, the NaI excited-state vibrational motion can be monitored, as well as the decay in the excited-state population due to nonadiabatic transitions from the decreasing gray intensity. For excitation of NaI with a room-temperature ground-state distribution of internuclear distances, large amplitude oscillations, with a period of ∼4 ps, are observed. This large amplitude vibrational motion arises from excitation of NaI around the inner turning point of NaI motion on the ground-state potential, and results in promotion of NaI onto a highly repulsive point of the excited-state potential. For long-lived clusters (cf. Figures 13c−f) even larger amplitude vibrational motion is observed, because the ionic branch of the excited state is lower in energy, relative to the gas phase, when a water molecule remains bound to excited NaI, and the outer-turning point for NaI motion on the excited state extends further out, as illustrated by the long tail in the NaI vibrational period distributions shown in Figure 6. The increase in the vibrational dephasing of NaI as a function of increasing cluster size is also quite obvious from the photoelectron spectra. Finally, the small amplitude vibrational motion caused by NaI energy transfer to evaporating water molecules in short-lived clusters, evidenced by the decrease in the average NaI vibrational period as a

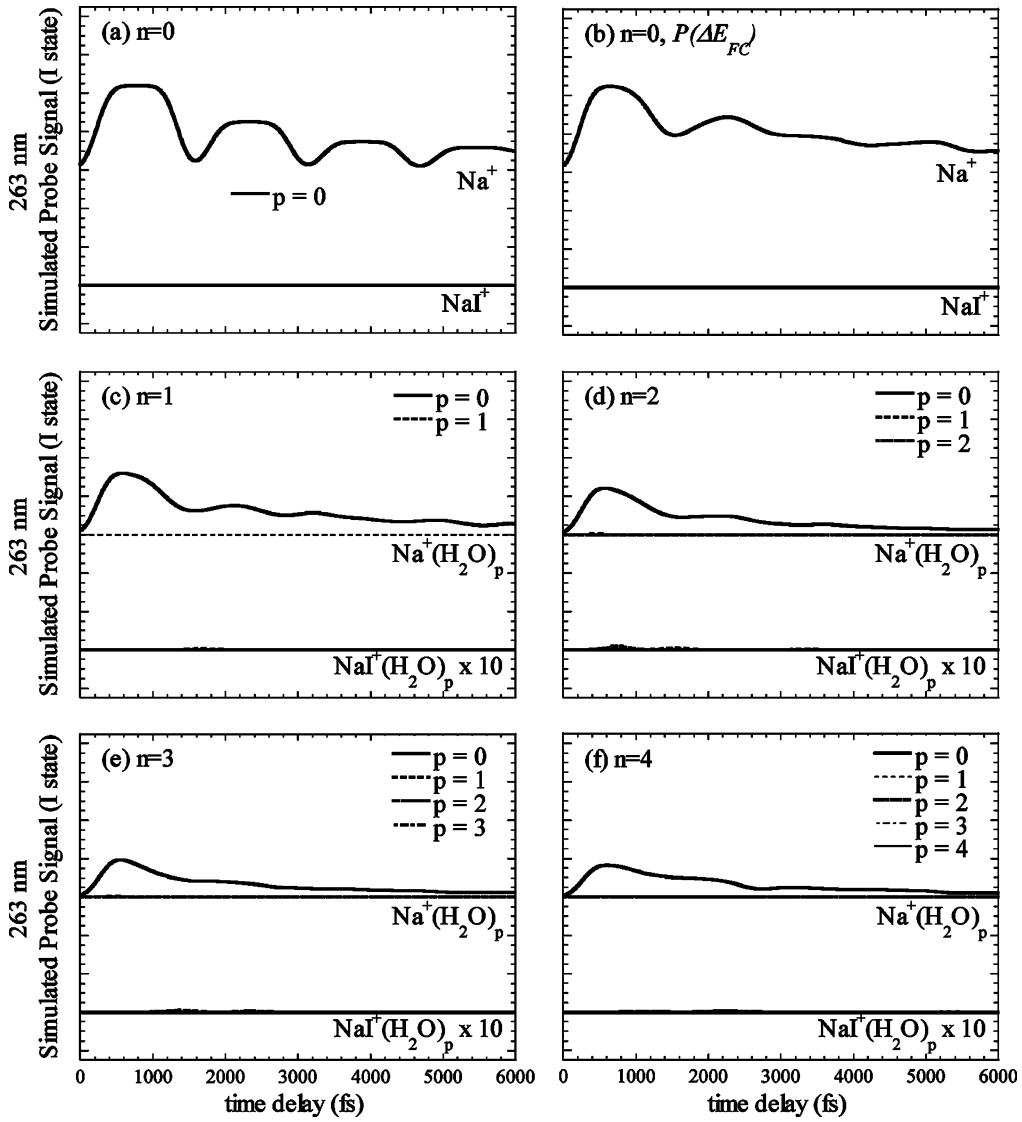

Figure 12. Probe signals for NaI$(H_2O)_n$ photodissociation as a function of pump−probe time delay, generated using a 263 nm excitation from the ionic branch of the NaI first excited state to the I probe state. The product cluster size p is 0 (solid), 1 (dash), 2 (dot), 3 (dash−dot) and 4 (thin solid). The $NaI^+(H_2O)_p$ probe signals have been magnified by a factor of 10 relative to the $Na^+(H_2O)_p$ signals due to the low intensity of the signals.

function of cluster size in Table 2, can also be observed in the photoelectron spectra. Therefore, the photoelectron spectra bring evidence of large amplitude NaI vibrational motion caused by the stabilization of the ionic branch of the excited state, further evidence of the enhancement in the excited-state NaI vibrational dephasing caused by the presence of an increasing number of surrounding water molecules, and small amplitude NaI vibrational motion due to energy transfer between NaI and evaporating water molecules.

IV. Concluding Remarks

We have investigated the photodissociation dynamics of NaI$(H_2O)_n$ [$n = 1-4$] clusters using a semiempirical valence-bond approach to describe the NaI electronic structure and classical solvent−solvent and solute−solvent interaction potentials, along with the molecular dynamics with quantum transitions method developed by Tully and co-workers.[54] Our simulations show that the excited-state population decay upon reaching the curve-crossing region increases with cluster size due to the increasing stabilization of the ionic branch of the NaI excited state by surrounding water molecules, and to multiple nonadiabatic transitions caused by dynamical fluctuations of the NaI internuclear separation at which the curve crossing occurs. After reaching the curve-crossing region for the first time, however, the excited-state population decay for all cluster sizes resembles that of bare NaI, although the periodicity of the NaI excited-state vibrational motion disappears in clusters due to vibrational dephasing. The excited-state population decay is no longer influenced by the water molecules beyond the first time NaI reaches the curve-crossing region because of rapid evaporation of 99% and 95% of the water population for NaI(H_2O) and NaI$(H_2O)_n$ [$n = 2-4$], respectively. The rapid water evaporation, which is governed by highly repulsive forces due to the reversed NaI polarity in the Franck−Condon region of the first excited state, takes place before internal vibrational energy redistribution and is thus nonstatistical. Furthermore, analysis of the post-evaporation water energy distributions revealed that the initial impulsive dynamics results in extensive rotational excitation, such that product water molecules are formed more rotationally than translationally hot, further supporting the highly nonstatistical nature of the water evaporation process. Successful comparison of NaI$(H_2O)_n$ excited-state forces predicted by our QM/MM model to those obtained from high-level ab initio calculations confirms that our simulation methodology yields

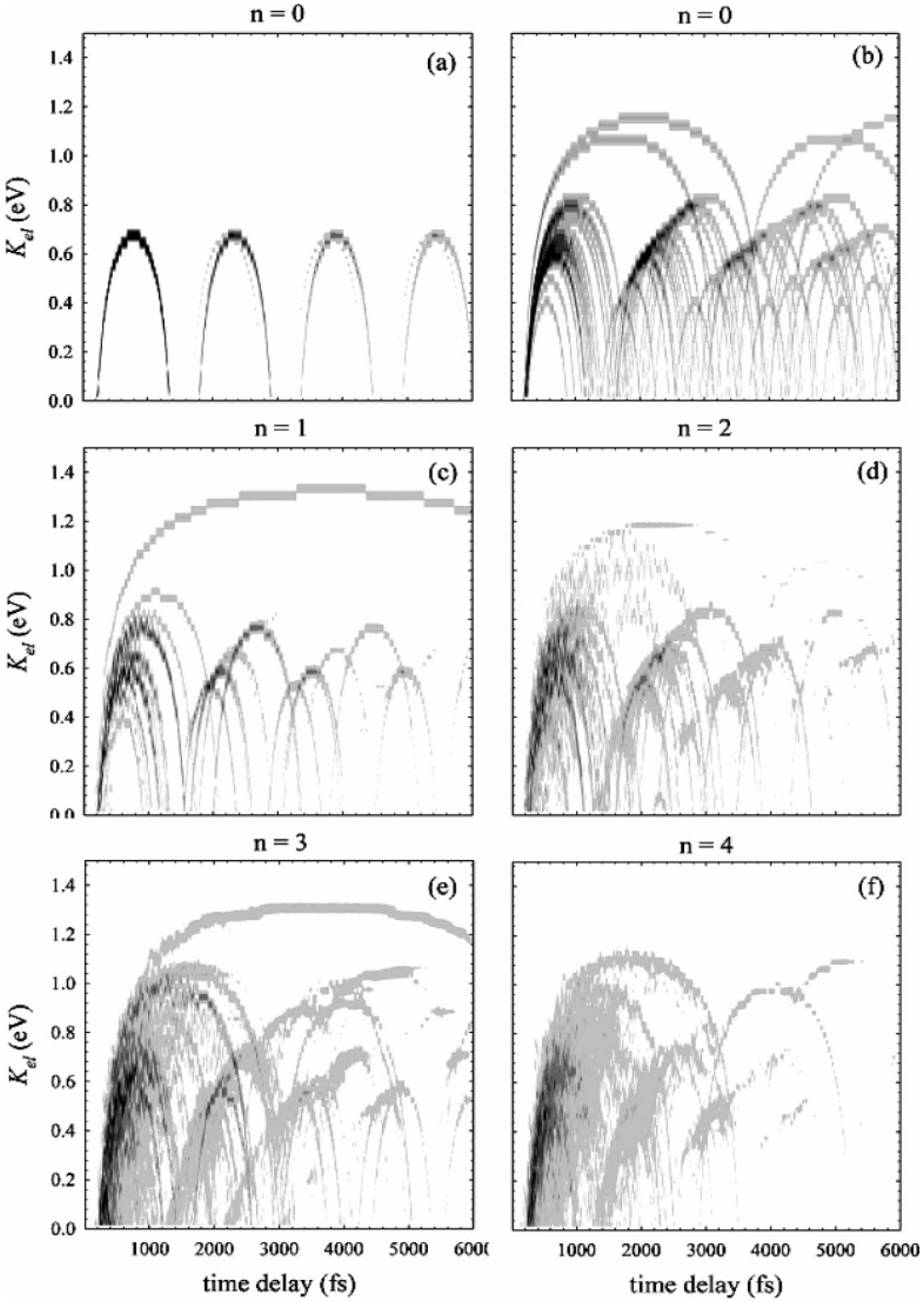

Figure 13. Time-resolved photoelectron spectra, produced with the one-photon detection scheme, as a function of pump−probe time delay. The gray scale is indicative of the NaI excited-state population, where the decreasing gray intensity corresponds to a decrease in the excited-state population.

realistic dynamics and water evaporation is a real feature of $NaI(H_2O)_n$ dynamics.

Our simulation results suggest that for 5% of the water population, in clusters containing 2−4 water molecules, solvent molecules remain transiently or permanently bound, mainly to the Na end of NaI. One or two water molecules may remain bound if NaI remains predominantly ionic (i.e., does not dissociate to atoms via a nonadiabatic transition) after reaching the curve-crossing region, and if the excess Franck−Condon energy in the NaI internuclear coordinate, gained from pump excitation, has already been depleted by the evaporation of neighboring water molecules. The vibrational period of NaI in the excited state may then extend beyond that of gas-phase NaI, due to stabilization of the ionic branch of the excited state, when water molecules remain bound to NaI after reaching the curve-crossing region. Finally, whereas water molecules retain the rotational energy gained from the initial repulsive dynamics, for long-lived clusters, energy is further transferred from NaI primarily to the water translational degrees of freedom.

High-level ab initio calculations have shown that both the NaI^+ X and I probe states are energetically accessible under the conditions employed in previous femtosecond pump−probe experiments.[62] In this work, we have considered excitation to both of these states and have simulated the $Na^+(H_2O)_p$ and NaI^+-

$(H_2O)_p$ probe signals resulting from two different schemes: a two-photon probe scheme used in previous femtosecond experiments of NaI photodissociation in water clusters,[24] where promotion to the probe state occurs from the covalent branch of the excited state, and a one-photon probe scheme employed in femtosecond studies of bare NaI,[15] where excitation occurs from the ionic branch of the excited state. In agreement with experimental findings, the $Na^+(H_2O)_p$ two-photon probe signals decay exponentially over the first NaI excited-state vibrational period with very little evidence of long-time dynamics. However, a strong bare Na^+ signal and a residual $Na^+(H_2O)$ signal are mostly obtained for all parent cluster sizes because excitation occurs to the repulsive wall of the probe state, causing further water evaporation. This clearly shows that experimentally observed signals arose from photodissociation of much larger parent clusters, because of the key role that water evaporation plays in the $NaI(H_2O)_n$ dynamics. On the other hand, the $NaI^+(H_2O)_p$ signal, which was presumably not detected experimentally, is clearly reminiscent of the parent cluster size. At short pump−probe time delays, two-photon excitation from the covalent branch corresponds to an almost instantaneous multiphoton excitation from the ground state, and because the water molecules are mainly found on the Na^+ end of NaI in the ground state, they remain bound to Na^+ on the probe state. Nonetheless, the simulated probe signals obtained with the two-photon probe scheme are not revealing of the NaI photodissociation dynamics beyond the time NaI reaches the curve-crossing region for the first time and therefore do not provide valuable information on the influence of water molecules on NaI photodissociation dynamics.

The simulated probe signals resulting from the one-photon scheme, on the other hand, are much more revealing of the NaI photodissociation dynamics. Only a bare Na^+ signal is obtained for all parent cluster sizes due to further water evaporation on the probe state. The intensity of the Na^+ signal decreases with pump−probe time delay, due to nonadiabatic transitions, but the oscillatory motion evident in the signal for bare NaI disappears in water clusters due to NaI vibrational dephasing. Furthermore, the intensity of the Na^+ signal decreases with increasing parent cluster size following the increasing stabilization of the ionic branch of the excited state, and the resulting increase of the nonadiabatic transition probability. Faint $NaI^+(H_2O)_p$ are also detected, where the first peak corresponds to the parent cluster size, as was the case for the two-photon detection scheme, and the successive evaporation of water molecules with increasing pump−probe delay can be monitored. Therefore, the one-photon probe scheme may allow monitoring of the effects of solvation on the nonadiabatic transition dynamics and successive evaporation of water molecules. We also note that the one-photon probe scheme is not very sensitive to solvation in small clusters, in that the differential solvation between the ionic branch of the NaI first excited state and the probe states is very small (as water molecules are located on the Na^+ end of NaI in both cases) and probe excitation energies will remain the same over a range of cluster sizes. Time-resolved photoelectron spectra resulting from the ejection of an electron from sodium on the probe state were also simulated. The information obtained from the spectra complements the $NaI^+(H_2O)_p$ probe signals, in that the effects of solvation on the excited-state NaI vibrational motion can be monitored. These findings warrant further experimental investigation of $NaI(H_2O)_n$ photodissociation dynamics. Finally, the possibility of observing inverted regime electron transfer behavior for NaI in these small clusters mentioned in the Introduction is obviously thwarted by the extensive evaporation observed. Nonetheless, this possibility remains open if this evaporation could be prevented by means of studying these small clusters in, e.g., a matrix or a sufficiently dense buffer gas.

Acknowledgment. This research was supported by the Natural Sciences and Engineering Research Council (NSERC) of Canada, and National Science Foundation (NSF) grants CHE-9520619 and CHE-9981539 (Colorado State University), CHE-970049, CHE-0108314 and CHE-0417570 (University of Colorado). G.H.P. holds a Concordia University Research Chair, D.M.K. is the recipient of a Canada Graduate Scholarship and Concordia University Graduate Fellowships, and Q.K.T. is the recipient of Concordia University Graduate Fellowships. Calculations were performed at the Centre for Research in Molecular Modeling (CERMM), which was established with the financial support of the Concordia University Faculty of Arts & Science, the Ministère de l'Éducation du Québec (MEQ) and the Canada Foundation for Innovation (CFI).

References and Notes

(1) Berry, R. S. Optical spectra of the alkali halide molecules. In *Alkali Halide Vapors*; Davidovits, P., McFadden, D. L., Eds.; Academic: New York, 1979.

(2) Lovas, F. J.; Tiemann, E. *J. Phys. Chem. Ref. Data* **1974**, *3*, 609.

(3) Jordan, K. D. Structure of alkali halides: theoretical methods. In *Alkali Halide Vapors*; Davidovits, P., McFadden, D. L., Eds.; Academic: New York, 1979.

(4) Faist, M. B.; Johnson, B. R.; Levine, R. D. *Chem. Phys. Lett.* **1975**, *32*, 1. Faist, M. B.; Levine, R. D. *J. Chem. Phys.* **1976**, *64*, 2953.

(5) Rose, T. S.; Rosker, M. J.; Zewail, A. H. *J. Chem. Phys.* **1989**, *91*, 7415. Cong, P.; Roberts, G.; Herek, J. L.; Mohktari, A.; Zewail, A. H. *J. Chem. Phys.* **1996**, *100*, 7832.

(6) Rosker, M. J.; Rose, T. S.; Zewail, A. H. *Chem. Phys. Lett.* **1988**, *146*, 175. Rose, T. S.; Rosker, M. J.; Zewail, A. H. *J. Chem. Phys.* **1988**, *88*, 6672. Zewail, A. H. *J. Chem. Soc., Faraday Trans.* **1989**, *85*, 1221. Cong, P.; Mohktari, A.; Zewail, A. H. *Chem. Phys. Lett.* **1990**, *172*, 109. Mohktari, A.; Cong, P.; Herek, J. L.; Zewail, A. H. *Nature* **1990**, *348*, 225. Zewail, A. H. *Faraday Trans. Chem. Soc.* **1991**, *91*, 207. Zewail, A. H. *Femtochemistry − Ultrafast Dynamics of the Chemical Bond*; World Scientific: Singapore, 1994. Zewail, A. H. In *Femtosecond Chemistry*; Manz J., Wöste L., Eds.; VCH: New York, 1994; Vol. 1, p 15.

(7) Engel, V.; Metiu, H.; Almeida, R.; Marcus, R. A.; Zewail, A. H. *Chem. Phys. Lett.* **1988**, *152*, 1. V. Engel and H. Metiu, *J. Chem. Phys.* **1989**, *90*, 6116.

(8) Engel, V.; Metiu, H. *Chem. Phys. Lett.* **1989**, *155*, 77. Braun, M.; Meier, C.; Engel, V. *J. Chem. Phys.* **1996**, *105*, 530.

(9) Sakai, Y.; Miyoshi, E.; Anno, T. *Can. J. Chem.* **1992**, *70*, 309.

(10) Martinez, T. J.; Levine, R. D. *Chem. Phys. Lett.* **1996**, *259*, 252; *J. Chem. Phys.* **1996**, *105*, 6334.

(11) Alekseyev, A. B.; Liebermann, H. P.; Buenker, R. J.; Balakrishnan, N.; Sadeghpour, H. R.; Cornett, S. T.; Cavagnero, M. J. *J. Chem. Phys.* **2000**, *113*, 1514.

(12) Grice, R.; Herschbach, D. R. *Mol. Phys.* **1974**, *27*, 159.

(13) For a review of femtosecond spectroscopy, see: Dantus, M.; Zewail, A. H. *Chem. Rev.* **2004**, *104*, 1717, and Baskin, J. S.; Zewail, A. H. *J. Phys. Chem. A* **2001**, *105*, 3680.

(14) Veen, N. J. A. V.; Vries, M. S. D.; Sokol, J. D.; Baller, T.; Vries, A. E. D. *Chem. Phys.* **1981**, *56*, 81.

(15) Jouvet, C.; Martrenchard, S.; Solgadi, D.; Dedonder-Lardeux, C.; Mons, M.; Grégoire, G.; Dimicoli, I.; Piuzzi, F.; Visticot, J. P.; Mestdagh, J. M.; D'Oliveira, P.; Meynadier, P.; Perdrix, M. *J. Phys. Chem. A* **1997**, *101*, 2555.

(16) Peslherbe, G. H.; Bianco, R.; Hynes, J. T.; Ladanyi, B. M. *J. Chem. Soc., Faraday Trans.* **1997**, *93*, 977.

(17) Peslherbe, G. H.; Ladanyi, B. M.; Hynes, J. T. *J. Phys. Chem. A* **1998**, *102*, 4100.

(18) Kim, H. J.; Hynes, J. T. *J. Chem. Phys.* **1990**, *93*, 5194, 5211; **1992**, *96*, 5088. Bianco, R.; Juanos i Timoneda, J.; Hynes, J. T. *J. Phys. Chem.* **1994**, *98*, 12103. Juanos i Timoneda, J.; Hynes, J. T. *J. Phys. Chem.* **1991**, *95*, 10431. Fonseca, T.; Kim, H. J.; Hynes, J. T. *J. Mol. Liq.* **1994**, *60*, 161.

(19) Bianco, R.; Hynes, J. T. *J. Chem. Phys.* **1995**, *102*, 7864; **1995**, *104*, 7885. For a review, see: Bianco, R.; Hynes, J. T. In *Solvent Effects and Chemical Reactivity*; Tapia, O., Bertrán, J., Eds.; Kluwer: Dordrecht, The Netherlands, 1996; p 259.

(20) See, e.g.: Hynes, J. T. *J. Phys. Chem.* **1986**, *90*, 3701 and references therein.
(21) Marcus, R. A. *J. Chem. Phys.* **1956**, *24*, 966; *J. Chem. Soc., Faraday Trans.* **1960**, *29*, 21.
(22) Grégoire, G.; Mons, M.; Jouvet, C.; Dedonder-Lardeux, C. *Eur. Phys. J. D* **1998**, *1*, 5.
(23) Grégoire, G.; Mons, M.; Dimicoli, I.; Dedonder-Lardeux, C.; Jouvet, C.; Martrenchard, S.; Solgadi, D. *J. Chem. Phys.* **1999**, *110*, 1521.
(24) Grégoire, G.; Dedonder-Lardeux, C.; Dimicoli, I.; Jouvet, C.; S., M.; Solgadi, D. *J. Chem. Phys.* **2000**, *112*, 8794.
(25) Peslherbe, G. H.; Ladanyi, B. M.; Hynes, J. T. *J. Phys. Chem. A* **2000**, *104*, 4533.
(26) Peslherbe, G. H.; Ladanyi, B. M.; Hynes, J. T. *Chem. Phys.* **2000**, *258*, 201.
(27) Perera, L.; Berkowitz, M. L. *J. Chem. Phys.* **1991**, *95*, 1954, 4236; **1993**, *99*, 4236; **1993**, *99*, 4222. Dang, L. X.; Garrett, B. C. *J. Chem. Phys.* **1993**, *99*, 2972. Dang, L. X.; Smith, D. E. *J. Chem. Phys.* **1993**, *99*, 6950.
(28) Serxner, D.; Dessent, C. E. H.; Johnson, M. A. *J. Chem. Phys.* **1996**, *105*, 7231. Ayotte, P.; Bailey, C. G.; Weddle, G. H.; Johnson, M. A. *J. Phys. Chem. A* **1998**, *102*, 3067.
(29) Koch, D. M.; Peslherbe, G. H. *Chem. Phys. Lett.* **2002**, *359*, 381.
(30) Jungwirth, P.; Tobias, D. J. *J. Phys. Chem. B* **2002**, *106*, 6361.
(31) Zeiri, Y.; Shapiro, M. *Chem. Phys.* **1978**, *31*, 217. Shapiro, M.; Zeiri, Y. *J. Chem. Phys.* **1979**, *70*, 5264. Zeiri, Y.; Shapiro, M. *J. Chem. Phys.* **1981**, *75*, 1170.
(32) Zeiri, Y.; Balint-Kurti, G. G. *J. Mol. Spectrosc.* **1983**, *99*, 1.
(33) Mulliken, R. S. *J. Chim. Phys.* **1949**, *46*, 497, 675. Pariser, R. *J. Chem. Phys.* **1953**, *21*, 568. Pohl, H. A.; Rein, R.; Appel, K. *J. Chem. Phys.* **1964**, *41*, 3383.
(34) Atkins, P. W. *Molecular Quantum Mechanics*; Clarendon: Oxford, U.K., 1970.
(35) McGlynn, S. P.; Vanquickenborne, L. G.; Kinoshita, M.; Carroll, D. G. *Introduction to Applied Quantum Chemistry*; Holt, Rinehart and Winston: New York, 1972.
(36) Mulliken, R. S.; Rieke, C. A.; Orloff, D.; Orloff, H. *J. Chem. Phys.* **1949**, *17*, 1248.
(37) *CRC Handbook of Chemistry and Physics*, 77rd ed.; Lide, D. R., Ed.; CRC: Boca Raton, FL, 1996.
(38) Rittner, E. S. *J. Chem. Phys.* **1951**, *19*, 1030.
(39) Delvigne, G. A. L.; Los, J. *Physica* **1973**, *67*, 166.
(40) Schaefer, S. H.; Bender, D.; Tiemann, E. *Chem. Phys. Lett.* **1982**, *92*, 273. Schaefer, H. S.; Bender, D.; Tiemann, E. *Chem. Phys.* **1984**, *89*, 65.
(41) Hanson, H. G. *J. Chem. Phys.* **1955**, *23*, 1391. Barker, J. R.; Weston, R. E. *J. Chem. Phys.* **1976**, *65*, 1427. Anderson, W. R.; Wilson, B. M.; Rose, T. L. *Chem. Phys. Lett.* **1977**, *48*, 284. Bower, R. D.; Chevrier, P.; Das, P.; Foth, H. J.; Polanyi, J. C.; Prisant, M. G.; Visticot, J. P. *J. Chem. Phys.* **1988**, *89*, 4478. Blum, H.; Lindner, J.; Tiemann, E. *J. Chem. Phys.* **1990**, *93*, 4556.
(42) Su, T.-M. R.; Riley, S. J. *J. Chem. Phys.* **1979**, *71*, 3194.
(43) Wang, J.; Blake, A. J.; McCoy, D. G.; Torop, L. *Chem. Phys. Lett.* **1990**, *175*, 225.
(44) See also Zichi, D. A.; Ciccotti, G.; Kapral, R.; Hynes, J. T. *J. Phys. Chem.* **1989**, *93*, 6261. Benjamin, I.; Barbara, P. F.; Gertner, B. J.; Hynes, J. T. *J. Phys. Chem.* **1995**, *99*, 7557.
(45) Jorgensen, W. L.; Chandrasekhar, J.; Madura, J. D.; Impey, R. W.; Klein, M. L. *J. Chem. Phys.* **1983**, *79*, 926.
(46) Jorgensen, W. L.; Severance, D. L. *J. Chem. Phys.* **1993**, *99*, 4233.
(47) Chandrasekhar, J.; Spellmeyer, D. C.; Jorgensen, W. L. *J. Am. Chem. Soc.* **1984**, *106*, 903.
(48) Dang, L. X.; Pettitt, B. M. *J. Phys. Chem.* **1987**, *91*, 3349.
(49) Calculations using the Multi-Reference singly and doubly excited Configuration Interaction method with a double-ζ basis set (MRCI/DZ) and a relaxed water geometry were performed with the MOLPRO package. MOLPRO is a package of ab initio programs written by H.-J. Werner and P. J. Knowles, version 2002.6, with contributions from R. D. Amos, A. Bernhardsson, A. Berning, P. Celani, D. L. Cooper, M. J. O. Deegan, A. J. Dobbyn, F. Eckert, C. Hampel, G. Hetzer, T. Korona, R. Lindh, A. W. Lloyd, S. J. McNicholas, F. R. Manby, W. Meyer, M. E. Mura, A. Nicklass, P. Palmieri, R. Pitzer, G. Rauhut, M. Schatz, H. Stoll, A. J. Stone, R. Tarroni, T. Thorsteinsson. An augmented correlation-consistent double-ζ aug-cc-pVDZ basis set was used for hydrogen and oxygen (Dunning, T. H., Jr. *J. Chem. Phys.* **1998**, *90*, 1007. Kendall, R. A.; Dunning, T. H., Jr.; Harrison, R. J. *J. Chem. Phys.* **1992**, *96*, 6796), a correlation-consistent core/valence polarized double-ζ cc-pCVDZ basis set was used for sodium (Woon, D. E.; Dunning, T. H., Jr. *J. Chem. Phys.* **1995**, *103*, 4572), and the ECP46MDF large-core pseudpotential and basis set (Stoll, H.; Metz, B.; Dolg, M. *J. Comput. Chem.* **2002**, *23*, 767) were used for iodine.
(50) Jasper, A. W.; Zhu, C.; Nangia, S.; Truhlar, D. G. *Faraday Discuss.* **2004**, *127*, 1.
(51) Toniolo, A.; Thompson, A. L.; Martinez, T. J. *Chem. Phys.* **2004**, *304*, 133.
(52) Chen, F.; McCoy, A. B. *J. Phys. Chem. A* **2004**, *108*, 8819.
(53) Yu, N.; Margulis, C. J.; Coker, D. F. *J. Phys. Chem. B* **2001**, *105*, 6728.
(54) Tully, J. C. *J. Chem. Phys.* **1990**, *93*, 1061. Tully, J. C. *Int. J. Quantum Chem., Quantum Chem. Symp.* **1991**, *25*, 299. Hammes-Schiffer, S.; Tully, J. C. *J. Chem. Phys.* **1994**, *101*, 4657.
(55) Press: W. H.; Teukolsky, S. A.; Vetterling, W. T.; Flannery, B. P. *Numerical Recipes, the Art of Scientific Computing*, 2nd ed.; Cambridge University Press: Cambridge, England, 1992.
(56) Alternative methods have been reported to account for quantum decoherence [see ref 50]. We employ the original trajectory swarm methodology, in the present work, for simplicity.
(57) See, e.g.: Bala, P.; Grochowski, P.; Lesyng, B.; McCammon, J. A. *J. Phys. Chem.* **1996**, *100*, 2535. Schwartz, B. J.; Bittner, E. R.; Prezhdo, O. V.; Rossky, P. J. *J. Chem. Phys.* **1996**, *104*, 5942. Coker, D. F. In *Computer Simulation in Chemical Physics*; Allen, M. P., Tildesley, D. J., Eds.; Kluwer Academic Publishers: The Netherlands, 1993; p 315.
(58) For a discussion of the Hellmann−Feynman forces in *first-principles* or mixed quantum/classical MD simulations, see, e.g.: Bolton, K.; Hase, W. L.; Peslherbe, G. H. In *Multidimensional Molecular Dynamics Methods*; Thompson, D. L., Ed.; World Scientific: Singapore, 1998.
(59) Hellmann, J. *Einführung in die Quantenchemie*; Deuticke & Co.: Leipzig, 1937. Feynman, R. P. *Phys. Rev.* **1939**, *56*, 340.
(60) Swope, W. C.; Andersen, H. C.; Berens, P. H.; Wilson, K. R. *J. Chem. Phys.* **1982**, *76*, 637.
(61) Verlet, L. *Phys. Rev.* **1967**, *159*, 98.
(62) Timerghazin, Q. K.; Koch, D. M.; Peslherbe, G. H. *J. Chem. Phys.*, submitted for publication.
(63) Xie, J.; Zare, R. N. *J. Chem. Phys.* **1992**, *97*, 2891.
(64) Nosé, S. *Mol. Phys.* **1984**, *52*, 255.
(65) Ciccotti, G.; Ryckaert, J. P. *Comput. Phys. Rep.* **1986**, *4*, 345.
(66) Dzidic, J.; Kebarle, P. *J. Phys. Chem.* **1970**, *74*, 1466.
(67) Kebarle, P. *Annu. Rev. Phys. Chem.* **1977**, *28*, 445.
(68) Hiraoka, K.; Mizuse, S.; Yamabe, S. *J. Phys. Chem.* **1988**, *92*, 3943.